Macrophage-derived VEGF-C decreases hematogenous metastatic dissemination by normalizing the tumor vasculature

Sabrina de Souza Ferreira[1], Tatjana Wallmann[1*°] Thomas Kerzel[2°], Majken Wallerius[1], Margarita Bartish[1], Laura-Sophie Landwehr[1], Yangxun Pan[1], Dennis Alexander Agardy[1], Jonas Bergh[1], Johan Hartman[1,3], Mario Leonardo Squadrito[2*] and Charlotte Rolny[1#*].

[1]Karolinska Institute, Department of Oncology-Pathology, Stockholm, Sweden
[2]San Raffaele Telethon Institute for Gene Therapy (TIGET), Universitá Vita-Salute San Raffaele, Milan, Italy.
[3]Department of Clinical Pathology and Cytology, Karolinska University Laboratory, Stockholm, Sweden.

*Equal Contribution
[#]Corresponding author: Charlotte Rolny, Karolinska Institutet, Department of Oncology-Pathology, SciLifeLab, Solna 171 76 Stockholm, Phone: +46(0)8-517 76 882, e-mail: charlotte.rolny@ki.se

Running Title: VEGF-C normalizes the tumor vasculature

Keywords: Vascular Endothelial Growth Factor-C, Tumor-Associated Macrophages, hypoxia, vascular normalization, metastatic dissemination, TMEM score.

Conflicts of interest: JH obtained speaker's honoraria or advisory board remunerations from Roche, Novartis, AstraZeneca, Eli Lilly. None of the other authors have a conflict of interest to disclose.

Total number of words: 6136; Figures: 5

ABSTRACT

Expression of pro-lymphangiogenic vascular endothelial growth factor (VEGF)-C in the primary tumor correlates with the occurrence of proximal lymph node metastasis in most solid cancer types, including those of the breast. However, the role of VEGF-C in regulating tumor cell dissemination to distant organs, such as the lungs, is currently unclear. Perivascular tumor-associated macrophages (TAMs) are key regulators of hematogenous tumor cell spreading, forming tumor microenvironment of metastasis (TMEM) doorways for breast cancer cells to intravasate tumor blood vessels and fuel distant metastases. Using an experimental breast cancer (BC) model, we show here that TAMs expressing VEGF-C decrease tumor cell dissemination to the lung. The mechanism by which TAM-derived VEGF-C hampered pulmonary metastases involved a phenotypic change in the TAMs, which upregulated the expression of Podoplanin and LYVE1, concomitant with augmented VEGFR3 expression on blood vessels, leading to vessel normalization and improved vessel functionality. We obtained evidence that TAM-derived VEGF-C may play a role in hematogenous spreading also in human breast cancer; indeed, perivascular TAMs expressing VEGF-C inversely correlated with the malignant grade and TMEM assembly. Thus, our study reveals an apparently paradoxical role of TAM-derived VEGF-C in regulating hematogenous tumor spreading in both experimental models and clinical samples.

SIGNIFICANCE STATEMENT

Pro-angiogenic tumor-associated macrophages (TAMs) are key drivers for metastatic dissemination. Here, we unravel that, TAM-derived VEGF-C facilitates tumor vessel normalization and functionality coinciding with a decrease in pulmonary metastasis. In line with our experimental data, expression of VEGF-C by perivascular TAMs correlates inversely with malignant grade and the occurrence of tumor microenvironment of metastasis (TMEM) complexes in a cohort of breast cancer specimens. Thus, our study reveals paradoxical roles of VEGF-C that should be taken into consideration upon using VEGF-C expression for prognosis.

INTRODUCTION

BC is one of the most prevalent cancers worldwide. While the prognosis for non-macrometastatic BC is generally good due to efficient adjuvant therapies, including targeted and endocrine therapy, the prognosis for metastatic BC or triple-negative breast cancer (TNBC), is much worse partly due to therapy resistance (1). New treatment strategies and biomarkers for these patients are therefore required.

Lymphangiogenic factors, including VEGF-C, promote tumor lymphangiogenesis and disrupts the lymph endothelial barrier (2) via its receptor VEGFR3, facilitating lymphatic invasion and tumor cell dissemination to the sentinel lymph nodes (3). The expression of VEGF-C in the primary tumor has thus been associated with the occurrence of lymph node metastasis for many solid human cancers including that of the breast (4). The occurrence of tumor-draining lymph node metastasis is a prognostic indicator for systemic tumor spread and is linked to poor clinical outcomes (5). However, it is still controversial to what extent BC cell colonization of distant organs occurs through lymphatic spreading from lymph node metastases (6). For example, experimental techniques such as carcinoma cell infusion into lymph nodes (7) or cancer cell photoconversion (8), indicated that a considerable proportion of lung metastases are formed by lymph node-derived cancer cells. Still, by performing genetic analyses of clonal evolution between the primary tumor, lymph node metastases, and distant metastases in human breast cancer, we showed that tumor cells residing at distant sites stem from the primary tumor and not from the sentinel lymph nodes (9), suggesting that BC cells disseminate mainly via the hematogenous route to colonize distant organs.

Abnormal expression of VEGF-A results in atypical tumor vessels that are usually irregular, disorganized, permeable, and leaky facilitating cancer cell intravasation into blood vessels (10). In contrast, normalization of the tumor vasculature is characteristically featured by enhanced vessel perfusion, reduced tumor hypoxia and increased pericyte coating of tumor vessels, resulting in hampering of distant metastasis (11). Tumor Associated Macrophages (TAMs) are a major source of VEGF-A that when located in the vicinity of tumor vessels act as "doorways" for cancer cells to intravasate blood vessels and fuel the occurrence of distant metastasis (12). These micro-anatomical structures are called tumor microenvironment of metastasis (TMEM) and are composed of a tumor cell expressing the actin-regulatory protein Mammalian-enabled (MENA), a perivascular macrophage and an endothelial cell (12-15). The density of TMEM has been shown to correlate with the occurrence of distant metastases in experimental mammary tumor models (12) and BC patients (13-15). For this reason, reprograming pro-angiogenic to angiostatic TAM has been shown to be a promising anti-metastatic strategy as shown by us (16, 17) and others (18).

As TAMs dominate the immune landscape of BC (19), we speculated that TAM-derived lymphangiogenic factors such as VEGF-C might regulate the route of metastatic dissemination. Indeed, we observed in our experimental model that TAM-derived VEGF-C increased sentinel lymph node metastasis, however, unexpectedly distant pulmonary

metastases were decreased. The mechanism whereby TAM-derived VEGF-C hampered pulmonary mechanism was ascribed to a phenotypic change of TAMs concomitant with augmented VEGFR3 expression on tumor vessels facilitating tumor vessel normalization and functionality. These data were substantiated in a cohort of ER^+ BC patients, showing that TAM-derived VEGF-C correlates inversely with BC malignant grade and the number of TMEM complexes. In sum, we propose a mechanism whereby TAM-derived VEGF-C attenuates pulmonary metastasis via the increased VEGFR3 expression of tumor vessels, mediating vascular normalization and hampering cancer cell intravasation.

RESULTS

VEGF-C is highly expressed in TAMs of 66cl4 tumors but not of 4T1 tumors

To elucidate the mechanism underlying the propensity of cancer cells to preferentially colonize lungs or lymph nodes, we employed 4T1 and 66cl4 murine BC cell lines that are derived from a single mouse mammary tumor but display different propensities to disseminate to lymph nodes and distant organs (20). For instance, 4T1 cancer cells preferentially disseminate to the lungs while 66cl4 cancer cells predominantly metastasize to lymph nodes (20, 21) and (**Fig. 1A).** In short, metastatic foci were determined by subjecting lungs and lymph node single suspensions to 6-thioguanine, for which both 4T1 and 66cl4 cells carry the resistance gene. The metastatic index was calculated by the number (#) of cancer cell colonies per tumor weight [gram (g)]. Both cell lines display features of human TNBC, *i.e.,* absence of estrogen and progesterone receptors, as well as amplification of *Erb-B2* [(a gene homologous to Human Epidermal Growth Factor Receptor 2, HER2)]. We next investigated the abundance of blood vessels and of lymphatic vessels in the two tumor models by using the blood endothelial cell marker CD31 and the lymph endothelial cell marker VEGFR3. Of note, a minor part of blood tumor vessels may also express VEGFR3 albeit at low levels (22). 66cl4 tumors did indeed display higher accumulation of lymphatic ($VEGFR3^+CD31^-$) vessels, as compared to 4T1 tumors in the tumor periphery (**Fig. 1B, C).** Unexpectedly, the majority of the 66cl4 blood tumor vessels also expressed VEGFR3 as compared to 4T1 tumors (**Fig. 1D, E).** Lymphangiogenesis was further evaluated by staining tumor sections for the two lymphatic markers LYVE1 and Podoplanin. Unexpectedly, a major part of 66cl4-infiltrating TAMs but not 4T1-TAMs expressed LYVE1 (**Fig. 1F, G**) and Podoplanin (**Suppl. Fig. 1A, B**) making these markers unsuitable for lymph vessel characterization. Due to that Podoplanin (23) and/or LYVE1 (24) expressing TAMs have been ascribed to be of a pro-lymphangiogenic phenotype and drive lymph node metastasis (23, 24), we next investigated if 66cl4-infiltrating TAMs displayed elevated levels of the pro-lymphangiogenic factor VEGF-C. Indeed, immunostaining

showed that VEGF-C was expressed by 66cl4-infiltrating TAMs to a markedly higher extent as compared to 4T1-infiltrating TAMs (**Fig. 1H, I**). qPCR analysis of flow cytometry-based sorted F4/80$^+$TAMs further verified that 66cl4-derived TAMs express elevated levels of *Vegfc* as compared to 4T1-derived TAMs (**Fig. 1J)**. In contrast, flow cytometry sorted GFP$^+$66cl4 and GFP$^+$4T1 cancer cells displayed similarly low levels of *Vegfc* that were prominently lower than 66cl4 TAMs (**Fig. 1J)**. Further analysis revealed that the pro-angiogenic factor VEGF-A expression was markedly higher in 4T1-cancer cells and -infiltrating TAMs as compared to 66cl4-cancer cells and infiltrating TAMs **(Suppl. Fig. 1C**). This was reflected by increased tumor vessel area in 4T1 tumors as compared to the 66cl4 tumors (**Suppl. Fig. 1D**). The 4T1-tumor vessels also appeared to be more abnormal as they were less covered by neural/glial antigen 2 (NG2)-positive and/or α-smooth muscle actin (α-SMA)-positive pericytes as compared to the 66cl4 model (**Suppl. Fig. 1E, F)**. Collectively, these data indicate that 66cl4-derived TAMs display elevated levels of VEGF-C, Podoplanin and LYVE1, coinciding with increased number of lymph node metastases and apparent normalized VEGFR3$^+$ tumor vessels that concomitantly display elevated VEGFR3 expression.

4T1 infiltrating TAMs expressing VEGF-C hamper pulmonary metastases

From the above data, we hypothesized that TAM-derived VEGF-C could normalize tumor vessels, thereby hampering distant metastatic dissemination. We therefore generated chimeric mice harboring haemopoietic cells, including TAMs, overexpressing VEGF-C. To this end, we transduced hematopoietic stem/progenitor cells (HSPCs) with lentiviral vectors (LVs) either empty (*Ctr*) or encoding for *Vegfc* that were then transplanted into recipient mice (denoted CTR and VEGF-C chimeric mice, respectively) that had undergone myeloablation, achieved by busulfan treatment (25). Upon hematopoietic reconstitution (6 weeks), 4T1 cells were injected into the fat pad of the chimeric mice (visualized in **Suppl. Fig. 2A**). LV efficiency was estimated by subjecting bone marrow (BM) cells derived from CTR and VEGF-C chimeric mice to qPCR showing an average of 2 integrated lentiviral vector copies per mouse genome (**Suppl. Fig. 2B**), which corresponded to that ~80 % of all 4T1-infiltrating TAMs expressed VEGF-C (**Fig. 2A, B**). Of note, we could not detect VEGF-C expression in immune cells apart from TAMs by using immunofluorescence for the pan-hemopoietic marker CD45 (**Fig. 2A, B**). VEGF-C protein expression in BM-derived macrophages (BMDMs) obtained from transplanted CTR and VEGF-C chimeric mice was further confirmed by western blot (**Suppl. Fig. 2C**). Importantly, transduction of HSPCs with *Vegfc* LVs did not affect *Vegfa* gene expression in BMDMs (**Suppl. Fig. 2D).**

Overexpression of VEGF-C in TAMs did not modify 4T1 tumor growth rate (**Fig. 2C**) nor the final tumor burden (**Suppl. Fig. 2E**) but did increase the occurrence of lymph node metastases

(**Fig. 2D**). Unexpectedly, tumor bearing VEGF-C chimeric mice exhibited a decrease in pulmonary metastases by ~55% as compared to controls (**Fig. 2E, F**) and the number of circulating tumor cells (as detected by colony forming assays (**Suppl. Fig 2F**). The increased incidence of lymph node metastases in VEGF-C chimeric mice coincided with an augmented occurrence of lymphatic vessels (VEGFR3$^+$CD31) in the tumor periphery as compared to 4T1 controls **(Fig. 2G, I)**. Furthermore, enforced expression of VEGF-C in TAMs in the 4T1 model, elicited VEGFR3 expression on CD31$^+$ vessels in the tumor center as compared to controls (**Fig. 2H, J)** coinciding with decreased vessel CD31$^+$ area (**Fig. 2K),** whereas the number of blood vessels was moderately increased (**Suppl. Fig. 2G**) resulting in an apparent increased blood vessel density [# of vessels/vessel mm^2 **(Fig. 2L)**]. Also, a major part of TAMs derived from the VEGF-C tumor bearing chimeric mice expressed LYVE1 (**Fig. 2M, N**) and Podoplanin (**Suppl. Fig. 2H, I)** as compared to controls. In sum, these data suggest that VEGF-C induces a phenotypic change in TAMs concomitant with increased expression of VEGFR3 on blood vessels.

TAM-derived VEGF-C normalizes the tumor vasculature

Blood vessel normalization facilitates restriction of cancer cell invasion and pulmonary metastases (11, 16), and is associated with hallmarks of vessel normalization such as improved vessel perfusion, increased pericyte coverage as well as decreased tumor hypoxia (26). 4T1 tumor-bearing CTR and VEGF-C chimeric mice were injected with FITC-conjugated lectin (which will only label vessels with a blood flow) and the hypoxic marker pimonidazole hydrochloride (PIMO), intravenously and intraperitoneally respectively, before euthanasia. 4T1 tumor sections from the VEGF-C chimeric mice displayed a significantly higher number of lectin perfused blood vessels (**Fig. 3A, B**) and reduced tumor hypoxia (**Fig. 3C, D**) compared to controls. In line, TAM-derived VEGF-C increased the number of blood vessels that were covered with α-SMA and NG2 positive pericytes (**Fig. 3E, F**).

To substantiate the role VEGF-C expressing TAMs on vessel normalization, we employed a co-mingling assay (Suppl. Fig. 3A), which entails BMDMs transduced with either *Ctr* or *Vegfc* LVs are mixed in Matrigel with 4T1 cancer cells, and then injected subcutaneously into syngeneic mice. Implants were harvested 8 days post-injection (before the onset of the humoral immune system). Immunostaining revealed that VEGF-C-expressing TAMs augment number of vessels labeled with FITC-conjugated lectin (**Fig. 4A, B**), NG2$^+$ and α-SMA$^+$ pericyte coated tumor vessels (**Fig. 4C, D)**, and the number of CD31$^+$ vessels expressing VEGFR3 in the center of the tumor (**Fig. 4E, F**) as compared to controls. On the other hand, vessel permeability [measured by 70 kDa biotin-conjugated dextran (**Suppl. Fig. 3B, C**)] and hypoxic

areas were reduced in tumors derived from VEGF-C chimeric mice as compared to controls (**Fig. 4G, H**). As we cannot study distant metastases in this tumor model (distant metastases do not develop in 8 days), we evaluated the occurrence of TMEM complexes, which is associated with tumor cell invasion of blood vessels in seeding of distant metastasis in experimental breast cancer models (12, 14). In line, VEGF-C expressing TAMs did indeed decrease TMEM assembly as compared to controls (**Fig. 4I, J**). In summary, overexpression of VEGF-C in TAMs increased vessel normalization and functionality and decreased the TMEM score.

TAM-derived VEGF-C does not alter the tumor immune composition

Lymphatic vessels are extensively involved in regulating immune cell trafficking that may affect tumor growth and metastatic dissemination (6). We therefore investigated if TAM-derived VEGF-C could affect the intratumoral cellular immune composition by employing flow cytometry. VEGF-C overexpression in TAMs did not affect accumulation of total CD11b$^+$ myeloid cells (**Suppl. Fig. 4A**), CD11b$^+$F4/80$^+$ TAMs (**Suppl. Fig. 4B**), Ly6G$^+$ neutrophils (**Suppl. Fig. 4C**), Ly6C$^+$ monocytes (**Suppl. Fig. 4D**), immunostimulatory [also known as M1-like TAMs (**Suppl. Fig. 4E)**] or immunosuppressive TAMs [also known as M2-like TAMs (**Suppl. Fig. 4F**)]. Immunostimulatory TAMs were identified by high expression of F4/80$^+$, MHC class II, CD11c$^+$, CD80$^+$, CD86$^+$ and MHC class I$^+$ (**Suppl. Fig. 4E)** while immunosuppressive F4/80$^+$ TAMs were identified by low expression of MHC class II or elevated levels of mannose receptor c-type 1 (MRC1) (**Suppl. Fig. 4F**). Of note, BMDMs engineered to express VEGF-C did not display altered expression levels of immunostimulatory cytokines such as C-X-C motif ligand (*Cxcl)-9, -10 and -11, interleukin 1a (Il-1a),* or immunosuppressive factors including *Il-10, arginase1* (*Arg1*), *Mrc1* and *transforming growth factor* (*Tgfβ)*, detected by qPCR (**Suppl. Fig. 4G)**. This indicates that VEGF-C does not alter the activation or the polarization status of macrophages. Finally, TAM-driven VEGF-C did not affect the accumulation of T cells (neither total CD3$^+$ T cells nor CD4$^+$ and CD8$^+$ T cell subpopulations) or CD49b$^+$ NK cells (**Suppl. Fig. 4H**). Hence, these data show that enforced expression of VEGF-C in HSPCs does not affect the intratumoral immune composition or the TAM phenotype.

VEGF-C expressing TAMs inversely correlates to TMEM assembly and grade of malignancy in human breast cancer

Based on our experimental data, we speculated that perivascular TAM expressing VEGF-C may promote vessel normalization in human tumors and, therefore, be more frequent in low-grade BC as compared to high-grade BC. The majority of TNBC patient specimens that are available are of high-grade (i.e., grade 3, where the cancer cells are poorly differentiated and undergo rapid proliferation), therefore we focused on estrogen receptor (ER)-positive breast

cancer, which is also the most prevalent type in BC patients (~70 %) and, which can be targeted with endocrine therapy. However, half of the treated patients will develop metastatic disease within 20-years of diagnosis (27). Hence, we evaluated the accumulation of bulk and perivascular TAMs by immunostaining of tumor sections obtained from ER^+ ductal BC patient specimens of different histological grades (Nottingham Histological Grade I-III, where grade I and II indicates low grade, and grade III accounts for high grade). Bulk $CD68^+$ TAMs (**Fig. 5A, B**) and perivascular TAMs (**Fig. 5C**) accumulated to a higher extent in high-grade than in low-grade ER^+ BC. Additional immunofluorescence staining, which also included VEGF-C, revealed that both bulk TAMs (**Fig. 5D, E**) and perivascular TAMs expressed VEGF-C significantly higher in low-grade than in high-grade ER^+ BC (**Fig. 5D, F**).

As we lack information for distant metastases for this patient cohort, we evaluated the occurrence of TMEM assembly (a $MENA^+$ cancer cell, a $CD31^+$ endothelial cell and a $CD68^+$ TAM), a clinically validated prognostic marker for the occurrence of distant metastasis in BC patients (13, 28, 29). Immunofluorescence staining of TMEM assembly revealed that the TMEM score was significantly higher in high-grade than in low-grade ER^+ BC tumors (**Fig. 5G, H)** and correlated inversely with VEGF-C expressing TAM (**Fig. 5I).** In sum, these data indicate that the presence of TAMs expressing VEGF-C correlates inversely with TMEM assembly that enable hematogenic tumor cell dissemination in human BC.

DISCUSSION

TAMs are recognized as regulators of tumor progression and have been linked to poor clinical outcomes in most cancers (30). Like macrophages in many other tissues, TAMs show remarkable functional plasticity and often exhibit a spectrum of activation states that span from a immunostimulatory and anti-metastatic phenotype (sometimes referred to as M1-like) to an immunosuppressive and pro-metastatic (also referred to as M2-like) phenotype (31). Usually, TAMs will express markers characteristic of both activation states and their function will partly depend on their spatial localization (32). For instance, perivascular macrophages, such as the $TIE2^+$TAMs, promote angiogenesis (33) by secreting factors such as VEGF-A facilitating vessel permeability and cancer cell intravasation (12, 16). Perivascular TAMs are furthermore a part of the TMEM three-cell complex together with a MENA-expressing cancer cell and endothelial cells that function as gateways to hematogenous spreading (12-15, 28, 34).

VEGF-C expression in primary tumors correlates to lymph node metastasis for most solid cancer including those of the breast, colon, rectum, prostate, esophagus, stomach, lung, uterine cervix and the endometrium (35). However, the role of VEGF-C on distant metastasis

is less clear. VEGF-C stimulates lymphangiogenesis via activation of VEGFR3 but can also regulate angiogenesis by binding to VEGFR2/VEGFR3 heterodimers, expressed by blood vessels during embryogenesis, endothelial tip cells in adults and tumor blood vessels (36). Deletion of VEGFR3 in blood vessels enhances VEGFR2 expression that stimulates the VEGF-A/VEGFR2 pathway, resulting in excessive vascular permeability (22) and hyper sprouting (37). In contrast, TAM-derived VEGF-C maintain the maturation of VEGFR3 expressing blood vessels (37). We show here that VEGF-C expressing TAMs increase VEGFR3 expression on tumor vessels, concomitant with increase of vessel normalization and functionality resulting in hampering of pulmonary metastasis. We therefore hypothesize that perivascular VEGF-C$^+$ TAMs stimulate endothelial cells to express VEGFR3, in a local-dose dependent fashion, facilitating tumor vessel normalization. In contrast, lymphangiogenesis and dissemination to the lymph nodes was increased. Importantly, VEGF-C expression by TAMs did not alter their expression of pro-inflammatory or immunosuppressive cytokines nor did it affect the autocrine levels of VEGF-A. Further clinical relevance for VEGF-C expressing TAMs was established in a cohort of ER$^+$ BC specimens, as these TAMs correlated inversely with malignant grade and the TMEM assembly. Our results are paradoxical to the fact that VEGF-C levels in primary tumors and in serum correlates to malign tumors and lymph node metastases (3, 6). However, these levels might just be an indicative of malign disease rather than VEGF-C itself fuel the tumor cell seeding from the lymph nodes to distant organs. Collectively, our data show that TAM-derived VEGF-C plays an unexpected role in normalizing the tumor vasculature and decreasing hematogenous cancer cell spreading.

MATERIALS AND METHODS

Generation of VEGF-C vector

Vegfc ORF clone was purchased from Thermo Scientific Fisher and amplified by PCR (95 °C for 5 min, 5 cycles at 95 °C for 30 sec, 45 °C for 30 sec, 72 °C for 30 sec and 30 cycles at 95 °C for 30 sec, 68 °C for 30 sec, 72 °C for 30 sec). Primers for *Vegfc* amplification are FW 5'-TAAAGACCGGTCAAAAGTTGCGAGCC-3' and RW 5'-TCGGGGTCGACTACAATTTTCATTTTATTTTAAAC-3' primers. The DNA coding for *Vegfc* was then inserted into a CMV.GFP.WPRE lentiviral vector sequence as described previously (38) downstream to the CMV promoter.

Lentivirus production

Vesicular stomatitis virus-G protein (VSV-G)-pseudotyped lentivirus vectors either empty or encoding *Vegfc* were produced by transient five-plasmid co-transfection into HEK293T cells

and concentrated using ultracentrifugation as described previously (38). Lentiviral vector titers were determined on HEK293T cells by TaqMan analysis as described previously (38). Lentiviral vectors were resuspended in PBS and stored at -80 °C.

Cell culture

Tumor cell lines

HEK293T cells were grown in Dulbecco's Modified Eagle's Medium (DMEM) while 66cl4 and 4T1 mammary carcinoma cells were grown in RPMI-1640 medium (Gibco). Both the RPMI-1649 and the DMEM mediums were supplemented with 10% fetal bovine serum, 1% penicillin/streptomycin (Gibco) and 1% L-glutamine (Gibco). 4T1 and 66cl4 mouse mammary carcinoma cells were originally derived from a single spontaneous tumor that arose in a BALB/cfC3H mouse and were purchased from the Karmanos Cancer Institute at Wayne State University.

Generation of 4T1 cells expressing VEGF-C

1 x 10^6 4T1 cells were transduced with 1 x 10^8 TU/ml of empty vector or *Vegfc* LVs in the presence of polybrene (SIGMA).

Bone-marrow derived macrophages (BMDMs)

Bone marrow cells were acquired by flushing the femurs and tibias of female BALB/c mice as described before (39). Cells were cultured in RPMI-1640 medium (Gibco) supplemented with 10% fetal bovine serum, 1% penicillin/streptomycin (Gibco), 1% L-glutamine (Gibco) and 50 ng/ml M-CSF (Miltenyi biotech) for 8 days as described before (39).

gDNA isolation and quantitative RT-PCR

To evaluate the integration of the viral backbone into the hematopoietic progenitor cells, bone marrow cells of transplanted tumor bearing CTR and VEGF-C mice were isolated and gDNA was purified using QIAmp DNA Mini Kit (Qiagen) as described (37). Vector integration was determined by quantifying copy numbers of HIV normalized to housekeeping gene beta actin by quantitative RT-PCR (95 °C for 10min, 40 cycles at 95 °C for 15 sec and 60 °C for 1 min).

Quantitative PCR

Flow sorted 66cl4- and 4T1-tumor cells, 66cl4 and 4T1 infiltrating TAMs and BMDMs were collected in RLT buffer (Qiagen) and homogenized using a syringe with a 20G needle. RNA was extracted using the RNeasy Mini Kit (Qiagen) according to the manufacturer's instructions

and reverse-transcribed with the QuantiTect Reverse Transcription kit according to the manufacturer's instructions (Qiagen). Genomic DNA was eliminated using gDNA Wipeout Buffer (Qiagen) for 2 min at 42 °C. qPCR was performed using either TaqMan Universal MasterMix II and TaqMan Gene Expression Assays (Applied Biosystems) or SYBR™ Green PCR Master Mix (Applied Biosystems) in a total volume of 10 µL. The polymerase was activated at 95 °C for 10 min and the PCR was performed for 40 cycles (95 °C for 15 s and 60 °C for 60 s). Following TaqMan probes for the following genes were used: *Vegfa* (Mm01281449_m1), *Vegfc* (Mm00437310_m1), *Cxcl9* (Mm00434946_m1), *Cxcl10* (Mm00445235_m1), *Cxcl11* (Mm00444662_m1), *Il10* (Mm00439614_m1), *Arginase1* (Mm00475988_m1), *Mrc1* (Mm01329362_m1), *Tgfβ* (Mm01178820_m1) and *β-actin* (Mm00607939_s1) (Life Technologies).

Mouse Tumor experiments

Tumor inoculation

Female BALB/c mice (4-6 weeks old) were purchased from Charles River Laboratory. 2 x 10^5 4T1 cells were injected into the mammary fat pad of anesthetized animals. Tumor size was measured externally using calipers, and tumor volumes were estimated using the following equation: V_{sphere} = 4/3 π x (d/2) 2 x D/2 (d: minor tumor axis, D: major tumor axis). Mice were euthanized 3- to 4-weeks after tumor cell injection, and tumors were weighed after dissection. All ethical permits were obtained from the Swedish Board of Agriculture (N65/16 and 8525-2020).

Bone marrow transplant

Bone marrow cells were acquired by flushing the femurs and tibias of 6- to 8-week-old female BALB/c mice and treated with red blood cell lysis buffer (Sigma). Lineage negative hematopoietic stem and progenitor cells (HSPCs) were purified using EasySep Isolation Kit (StemCell Technologies) according to manufacturer's instructions. 2 x 10^6 lineage negative cells/ml were transduced with 1 x 10^8 TU/ml of empty vector or *Vegfc* lentivirus in serum-free StemSpan medium (StemCell Technologies) supplemented with 10 ng/ml IL-3, 20 ng/ml IL-6, 100 ng/ml SCF and 10 ng/ml FL-T3L (Stem Cell Technologies). 1 x 10^6 transduced HSPCs were resuspended in PBS and injected into the tail vein of 6-week-old female Balb/c mice, that had undergone myeloablation using 20 mg/kg Busulfan (Sigma) by intraperitoneal (i.p.) injection on three consecutive days. Busulfan was solubilized in DMSO and diluted to 5 mg/ml in PBS. On the fourth day 12–14 × 10^6 BM cells were given by tail vein injection. This procedure resulted in ~80 % chimerism as described (40).

Lung colony assay

Lungs and lymph nodes from tumor bearing mice were dissected into an enzymatic buffer, dissociated to single cell suspensions and cultured in RPMI-1640 (complete medium) supplemented with 60 μM 6-Thioguanine (Sigma) as previously described (21). Colonies formed by tumor cells resistant to 6-Thioguanine were fixed with 4% Formaldehyde (VWR Chemicals) and stained with Hematoxylin Harris (VWR Chemicals). Metastasis colonies were counted, and the metastatic index was calculated by using the equitation M_{index} = n/w (n: number of metastases, w: weight of tumor) (21).

Co-mingling assay

BMDM were transduced with 1 x 10^8 TU/ml of empty vector or *Vegfc* lentivirus vectors, 4 days post-differentiation as described (39). Two days after transduction, engineered BMDMs were then embedded in 200 μL of growth factor reduced Matrigel (BD Bioscience) together with 2 × 10^5 4T1 cancer cells, and injected subcutaneously into the flank of 8-week-old female BALB/c mice for 8 days.

Flow Cytometry

Single cell suspensions tumors were pre-incubated with anti-CD16/32 mAb (BioLegend) for 15 min on ice to prevent non-specific binding, with subsequent incubation with specific antibodies for 30 min on ice. Cells were stained using the following antibodies: CD11b (M1/70), CD45 (30-F11), Ly6C (AL-21), Ly6G (1A8), CD86 (GL1), CD11c (HL3), CD3 (500A2/145-2c11), CD8 (53-6.7), CD4 (RM4-5), CD49b (HM ALPHA2), MHC class II (I-A/I-E), MHC class I (H-2K(d)) and CD80 (16-10A1; all from BD Bioscience), F4/80 (BM8) and MRC1 (C068C2; BioLegend). The viability of cells was verified using 7-AAD (Life Technologies). Samples were acquired with a LSR II (BD Biosciences) and analyzed using FlowJo software (Tree Star).

Western Blot

Cells were lysed in NP-40 (Thermo Fisher Scientific) with freshly added Halt™ Protease Inhibitor Cocktail (Thermo Fisher Scientific). Protein concentrations were determined using the bicinchoninic acid (BCA) method (Thermo Fisher Scientific) according to the manufacturer's instructions. 20 μg of protein was incubated with antibodies against VEGF-C (Abd Serotec) for 2 h on ice before mixing with protein G-Sepharose (Thermo Fisher Scientific). The antibody complex was washed three times in lysis buffer and once in Tris-buffered saline (TBS). The beads were resuspended in sample buffer, boiled for 5 min, and subjected to electrophoresis in 10% or 4–12% Bis-Tris gels and transferred to nitrocellulose membranes using iBlot2 (Life technologies). Membranes were probed for VEGF-C (Santa Cruz) followed by horseradish

peroxidase-conjugated secondary antibodies (Life Technologies). Membranes were then washed and visualized with an enhanced chemiluminescence (ECL) detection system (GE Healthcare) and iBright CL1000 (Thermo Fisher Scientific). Signals were quantified using ImageJ software (NIH).

Immunofluorescence analysis

Tumors embedded in OCT, a cryo embedding matrix, were cut in 10 µm thick sections and fixed in methanol. Paraffin-embedded tumor sections were treated for antigen retrieval with sodium citrate buffer (Thermo Scientific Fisher). All tumor sections were blocked in blocking buffer containing PBS (Sigma), 0.3 % Triton X-100 (Sigma), 10 % fetal bovine serum (Gibco) and 1 % Bovine Serum Albumin (Sigma), and immunostained with the appropriate antibodies: anti CD68 (Dako), VEGF-A (SantaCruz), CD31 (BD Biosciences), Podoplanin (Life Technologies), LYVE-1 (Medical and Biological Laboratories), NG2 (Merck Millipore), α-SMA (Sigma-Aldrich), F4/80 (Bio-Rad), VEGF-C (Santa Cruz), VEGFR3 (R&D Systems), CD31 (DAKO), FITC-Lectin (Bio-Rad) and MENA/ENAH (Sigma). The appropriate secondary antibodies were conjugated with AlexaFluor 488, AlexaFluor 546, AlexaFluor 555 or AlexaFluor 647 fluorochromes (Life Technologies). Cell nuclei were labeled with DAPI (Invitrogen Corp). 10 independent fields from each section were analyzed by using LSM 710 Zeiss confocal microscope and quantified by ImageJ software.

Tumor hypoxia and vessel functionality

Tumor hypoxia was assessed by intraperitoneal injection of 60 mg/kg pimonidazole hydrochloride (Hypoxiprobe) into tumor-bearing mice. Mice were sacrificed 1 h after injection and tumors were harvested. To detect the formation of hypoxic adducts, OCT tumor sections were immunostained with Hypoxyprobe-1-Mab-1 (Hypoxiprobe kit, Chemicon) following manufacturer's instructions. Vessel perfusion was evaluated by intravenous injection of 1 mg of FITC-conjugated Lectin (Molecular Probes). Tumors were embedded in OCT material (VWR Chemicals) and snap-frozen in iso-pentane (VWR Chemicals) on dry ice.

Patient material

Paraffin-embedded whole tumor sections from breast cancer patients were obtained from Karolinska University Hospital and Southern Hospital, Stockholm, Sweden. All breast cancer patients at the Karolinska University Hospital and Southern Hospital have approved and signed a written consent for biobanking, including research purposes that have been approved by the local ethical committee (2016/957-31; *ex vivo* tumor models).

Statistical analysis

GraphPad Prism 6 software was used for graph/plot generation and statistical hypothesis testing. All data from representative experiments are presented with Standard Deviation (SD) and mean Statistical analyses were performed using Student's t-test, two-way ANOVA or one-way ANOVA as indicated in the figure legends. Stars and hashtags in the graphs indicate significance as depicted in the figure legends. Differences were considered statistically significant at $p<0.05$.

FINANCIAL SUPPORT

This study was supported by the Swedish Cancer Society (2016/825 and 2019/0281), Swedish Scientific Council (VR, 2018-02915 and 2021-01149), Radiumhemmets research funds (154352) to CR; Swedish Cancer Society and the Wallenberg foundation to JB; TW was supported by KI-PhD (2014-2018) foundation. JH was supported by grants from Radiumhemmets research funds, Swedish Breast Cancer Association, Swedish Society for Medical Research. MLS was supported by Fondazione Regionale per la Ricerca Biomedica (FRRB) 1751658-2020 and CARIPLO 1834-2019.

REFERENCES

1. A. G. Waks, E. P. Winer, Breast Cancer Treatment: A Review. *JAMA* **321**, 288-300 (2019).
2. C. Tacconi *et al.*, Vascular endothelial growth factor C disrupts the endothelial lymphatic barrier to promote colorectal cancer invasion. *Gastroenterology* **148**, 1438-1451 e1438 (2015).
3. L. C. Dieterich, M. Detmar, Tumor lymphangiogenesis and new drug development. *Adv Drug Deliv Rev* **99**, 148-160 (2016).
4. S. Jana, R. A. Muscarella, Jr., D. Jones, The Multifaceted Effects of Breast Cancer on Tumor-Draining Lymph Nodes. *Am J Pathol* **191**, 1353-1363 (2021).
5. Q. Ma, L. C. Dieterich, M. Detmar, Multiple roles of lymphatic vessels in tumor progression. *Curr Opin Immunol* **53**, 7-12 (2018).
6. T. V. Petrova, G. Y. Koh, Biological functions of lymphatic vessels. *Science* **369** (2020).
7. M. Brown *et al.*, Lymph node blood vessels provide exit routes for metastatic tumor cell dissemination in mice. *Science* **359**, 1408-1411 (2018).
8. E. R. Pereira *et al.*, Lymph node metastases can invade local blood vessels, exit the node, and colonize distant organs in mice. *Science* **359**, 1403-1407 (2018).
9. I. Ullah *et al.*, Evolutionary history of metastatic breast cancer reveals minimal seeding from axillary lymph nodes. *J Clin Invest* **128**, 1355-1370 (2018).
10. S. Goel, A. H. Wong, R. K. Jain, Vascular normalization as a therapeutic strategy for malignant and nonmalignant disease. *Cold Spring Harb Perspect Med* **2**, a006486 (2012).
11. M. Mazzone *et al.*, Heterozygous deficiency of PHD2 restores tumor oxygenation and inhibits metastasis via endothelial normalization. *Cell* **136**, 839-851 (2009).
12. A. S. Harney *et al.*, Real-Time Imaging Reveals Local, Transient Vascular Permeability, and Tumor Cell Intravasation Stimulated by TIE2hi Macrophage-Derived VEGFA. *Cancer Discov* **5**, 932-943 (2015).
13. T. E. Rohan *et al.*, Tumor microenvironment of metastasis and risk of distant metastasis of breast cancer. *J Natl Cancer Inst* **106** (2014).

14. G. S. Karagiannis *et al.*, Neoadjuvant chemotherapy induces breast cancer metastasis through a TMEM-mediated mechanism. *Sci Transl Med* **9** (2017).
15. P. S. Ginter *et al.*, Tumor Microenvironment of Metastasis (TMEM) Doorways Are Restricted to the Blood Vessel Endothelium in Both Primary Breast Cancers and Their Lymph Node Metastases. *Cancers (Basel)* **11** (2019).
16. C. Rolny *et al.*, HRG inhibits tumor growth and metastasis by inducing macrophage polarization and vessel normalization through downregulation of PlGF. *Cancer Cell* **19**, 31-44 (2011).
17. A. M. Georgoudaki *et al.*, Reprogramming Tumor-Associated Macrophages by Antibody Targeting Inhibits Cancer Progression and Metastasis. *Cell Rep* **15**, 2000-2011 (2016).
18. M. L. Squadrito *et al.*, miR-511-3p Modulates Genetic Programs of Tumor-Associated Macrophages. *Cell Rep* **1**, 141-154 (2012).
19. J. Wagner *et al.*, A Single-Cell Atlas of the Tumor and Immune Ecosystem of Human Breast Cancer. *Cell* **177**, 1330-1345 e1318 (2019).
20. C. J. Aslakson, F. R. Miller, Selective events in the metastatic process defined by analysis of the sequential dissemination of subpopulations of a mouse mammary tumor. *Cancer Res* **52**, 1399-1405 (1992).
21. A. Casazza *et al.*, Systemic and targeted delivery of semaphorin 3A inhibits tumor angiogenesis and progression in mouse tumor models. *Arterioscler Thromb Vasc Biol* **31**, 741-749 (2011).
22. K. Heinolainen *et al.*, VEGFR3 Modulates Vascular Permeability by Controlling VEGF/VEGFR2 Signaling. *Circ Res* **120**, 1414-1425 (2017).
23. P. Bieniasz-Krzywiec *et al.*, Podoplanin-Expressing Macrophages Promote Lymphangiogenesis and Lymphoinvasion in Breast Cancer. *Cell Metab* **30**, 917-936 e910 (2019).
24. S. Bron *et al.*, TIE-2-expressing monocytes are lymphangiogenic and associate specifically with lymphatics of human breast cancer. *Oncoimmunology* **5**, e1073882 (2016).
25. H. Lund *et al.*, Competitive repopulation of an empty microglial niche yields functionally distinct subsets of microglia-like cells. *Nat Commun* **9**, 4845 (2018).
26. R. K. Jain, Normalizing tumor microenvironment to treat cancer: bench to bedside to biomarkers. *J Clin Oncol* **31**, 2205-2218 (2013).
27. A. B. Hanker, D. R. Sudhan, C. L. Arteaga, Overcoming Endocrine Resistance in Breast Cancer. *Cancer Cell* **37**, 496-513 (2020).
28. M. H. Oktay *et al.*, Correlated immunohistochemical and cytological assays for the prediction of hematogenous dissemination of breast cancer. *J Histochem Cytochem* **60**, 168-173 (2012).
29. B. D. Robinson *et al.*, Tumor microenvironment of metastasis in human breast carcinoma: a potential prognostic marker linked to hematogenous dissemination. *Clin Cancer Res* **15**, 2433-2441 (2009).
30. D. G. DeNardo, B. Ruffell, Macrophages as regulators of tumour immunity and immunotherapy. *Nat Rev Immunol* 10.1038/s41577-019-0127-6 (2019).
31. A. Mantovani, F. Marchesi, A. Malesci, L. Laghi, P. Allavena, Tumour-associated macrophages as treatment targets in oncology. *Nat Rev Clin Oncol* **14**, 399-416 (2017).
32. M. Yang, D. McKay, J. W. Pollard, C. E. Lewis, Diverse Functions of Macrophages in Different Tumor Microenvironments. *Cancer Res* **78**, 5492-5503 (2018).
33. M. De Palma, C. Murdoch, M. A. Venneri, L. Naldini, C. E. Lewis, Tie2-expressing monocytes: regulation of tumor angiogenesis and therapeutic implications. *Trends Immunol* **28**, 519-524 (2007).
34. D. Entenberg *et al.*, Validation of an Automated Quantitative Digital Pathology Approach for Scoring TMEM, a Prognostic Biomarker for Metastasis. *Cancers (Basel)* **12** (2020).
35. S. Karaman, M. Detmar, Mechanisms of lymphatic metastasis. *J Clin Invest* **124**, 922-928 (2014).

36. T. Tammela *et al.*, Blocking VEGFR-3 suppresses angiogenic sprouting and vascular network formation. *Nature* **454**, 656-660 (2008).
37. T. Tammela *et al.*, VEGFR-3 controls tip to stalk conversion at vessel fusion sites by reinforcing Notch signalling. *Nat Cell Biol* **13**, 1202-1213 (2011).
38. M. De Palma, L. Naldini, Transduction of a gene expression cassette using advanced generation lentiviral vectors. *Methods Enzymol* **346**, 514-529 (2002).
39. M. Bartish *et al.*, MNK2 governs the macrophage antiinflammatory phenotype. *Proc Natl Acad Sci U S A* 10.1073/pnas.1920377117 (2020).
40. M. De Palma, M. A. Venneri, L. Naldini, In vivo targeting of tumor endothelial cells by systemic delivery of lentiviral vectors. *Human gene therapy* **14**, 1193-1206 (2003).

FIGURE LEGENDS

Figure 1. VEGF-C is highly expressed in TAMs derived from 66cl4 tumors but not 4T1 tumors.

66cl4 and 4T1 cancer cells were injected into the mammary fat pad of syngeneic mice.

A, The graph displays the metastatic index of lung and lymph node cancer cell colonies in lung or lymph nodes [number of cancer cell colonies in lungs or lymph nodes per gram (g) of tumor weight] of 4T1 and 66cl4 tumor bearing mice.

B–**E,** Immunofluorescence analysis by confocal microscopy of 66cl4 and 4T1 tumor sections immunostained for the blood vessel marker CD31 (green), the lymphatic vessel marker VEGFR3 (red) and DAPI (grey). Representative images from tumor periphery in (**B**) and tumor inner region in (**D**). Morphometric analysis of VEGFR3$^+$CD31$^-$ lymphatic vessel area in (**C**), and number VEGFR3$^+$CD31$^+$ blood vessels in (**E**)**.**

F-G, Immunofluorescence analysis by confocal microscopy of 66cl4 and 4T1 tumor sections immunostained for CD31 (blue), the pan-macrophage marker F4/80 (green), the lymphatic vessel marker LYVE-1 (red) and DAPI (grey). Representative images in (**F**) and percentage of TAMs expressing LYVE1 in (**G**).

H–**I,** Immunofluorescence analysis by confocal microscopy of 66cl4 and 4T1 tumor sections immunostained for F4/80 (green), VEGF-C (red) and DAPI (grey). Representative images in (**H**) and percentage of TAMs expressing VEGF-C in (**I**). qPCR analysis of *Vegfc* in flow cytometry-sorted TAMs or GFP$^+$ cancer cells from 4T1 and 66cl4 tumors in **(J)**.

Statistical analyses were performed by Students t-test in (**A,C,E,G,I**) and by one-way ANOVA in (**J**); *$p<0.05$, **$p<0.01$, ***$p<0.001$ and ****$p<0.0001$; $n>15$ mice/group; data values are presented as mean ± SD. Bars represent 100 µm in (**B**,**D**,**F**,**H**).

Figure 2. TAM-derived VEGF-C decreases pulmonary metastasis

4T1 cancer cells were injected into the mammary fat pad of syngeneic chimeric mice harboring haemopoietic cells engineered with *Vegfc* or *Ctr* lentiviral vectors.

A–**B,** Immunofluorescence analysis by confocal microscopy of 4T1 tumor sections immunostained for F4/80 (blue), CD45 (green), VEGF-C (red) and DAPI (grey). Representative images in (**A**) and percentage of TAMs that express VEGF-C in (**B**).

C–**E,** Tumor growth of 4T1 tumors is displayed in (**C**), lymph node colonies in (**D**) and lung colonies in (**E**). Per gram tumor weight (the metastatic index) was quantified in (**D**) and (**E**), respectively.

F, Histology analysis of MENA expressing tumors in lungs from tumor bearing mice are depicted in the pictograms (**left**) and metastatic index was quantified **(right**).

G–**L,** Immunofluorescence analysis of 4T1 tumor sections immunostained for CD31 (green), VEGFR3 (red) and DAPI (grey). Representative images from tumor periphery in (**G**) and tumor inner area in (**H**). Quantification of $VEGFR3^{+}CD31^{-}$ lymphatic vessels in (**I**), % of $VEGFR3^{+}CD31^{+}$ blood vessels in **(J)**, % of $CD31^{+}$ blood vessel area in (**K**) and tumor blood vessel density (# of vessels divided by vessel area per optic field) in (**L**)**.**

M–**N,** Immunofluorescence analysis by confocal microscopy of tumor sections immunostained for F4/80 (green), LYVE1 (red) and DAPI (grey). Representative images in (**M**) and percentage of $LYVE1^{+}F4/80^{+}$ TAMs in (**N**).

Statistical analyses were performed by Students t-test; *p<0.05; **p<0.01, ***p<0.001 and ****p<0.001; n>10 mice/group. All data values are shown as the mean ± SD. Bars represent 100 μm in (**A**, **F**, **G**, **H** and **M**).

Figure 3. TAM-derived VEGF-C normalizes the tumor vasculature

4T1 cancer cells were injected into the mammary fat pad of syngeneic chimeric mice harboring haemopoietic cells engineered with *Vegfc* or *Ctr* lentiviral vectors.

A–**D,** 4T1 tumors from mice were injected with FITC-lectin intravenously and PIMO intraperitoneally before sacrification. Representative images show immunostaining for CD31 (red), FITC-conjugated lectin (green) and DAPI (grey) in (**A**), PIMO (hypoxia) and DAPI (grey) in (**C**). Vessel perfusion is quantified in (**B**) and hypoxic area in (**D**).

E–**F,** Immunofluorescence analysis of 4T1 tumors immunostained for CD31 (blue), the pericyte markers α-SMA (red) and NG2 (green), and DAPI (grey). Representative images are shown in (**E**) and morphometric analysis of $NG2^{+}$ or α-SMA^{+} pericyte covered $CD31^{+}$ blood vessels in (**F**).

Statistical analyses were performed by Students t-test; *p<0.05, and **p<0.01; n>10 mice/group. All data values are shown as the mean ± SD. Bars represent 100 μm in (**A**,**C**,**E**).

Figure 4. TAM-derived VEGF-C induces vascular normalization and decreases the TMEM score

4T1 cancer cells were co-mingled in Matrigel with BMDMs previously transduced with C*tr* or *Vegfc* LVs and injected subcutaneously into syngeneic mice.

A–**B,** CTR and VEGF-C tumor bearing mice were injected with FITC-conjugated lectin before sacrification. Tumor slides were immunostained for CD31 (red), FITC-conjugated lectin (green) and DAPI (grey) in (**A**). Morphometric analysis of proportion of perfused vessels is shown in (**B**).

C–D, Immunofluorescence analysis of 4T1 tumors immunostained for CD31 (blue), the pericyte markers NG2 (green) and α-SMA (red), and DAPI (grey). Representative images are shown in (**C**) and morphometric analysis of $NG2^+$ or α-SMA^+ pericyte covered $CD31^+$ blood vessels in (**D**).

E–F, Representative images show immunostaining for CD31 (green), VEGFR3 (red) and DAPI (grey) of the tumor inner area in (**E**). Proportion $VEGFR3^+CD31^+$ blood vessels, quantified in (**F**).

G-H, CTR and VEGF-C tumor bearing mice were injected with PIMO before euthanasia. Representative images show immunostaining for PIMO (green) and DAPI (grey) in (**G**). Hypoxic area was quantified in (**H**).

I–**J,** Immunostaining for CD31 (blue), F4/80 (green), MENA (red) and DAPI (grey) identified TMEM assembly (white arrows) in (**I**). The TMEM score was assessed in 20 high-magnification fields/whole tumor section (**J**).

Statistical analyses were performed by Students t-test; $^{**}p<0.01$ and $^{***}p<0.001$; n>10 mice/group. All data values are shown as the mean ± SD. Bars represent 100 μm in (**A,C**), 50 μm in (**E**) and 20 μm in (**I**).

Figure 5. TAM-derived VEGF-C inversely correlates to the grade of malignancy in human breast cancer and density of TMEM

A–**C,** Immunofluorescence analysis by confocal microscopy of human ER^+ breast tumors immunostained for CD31 (blue); pan-macrophage marker CD68 (green) and nuclei (DAPI; grey). Representative images in (**A**), quantitative analysis of $CD68^+$TAMs in (**B**) and $CD68^+$ perivascular TAMs in (**C**).

D–**F,** Immunofluorescence analysis by confocal microscopy of human ER^+ breast tumors immunostained for CD31 (blue), CD68 (green), and VEGF-C (red). Representative images in (**D**) and quantitative analysis of VEGFC expressing bulk TAMs in (**E**) and perivascular TAMs in (**F**).

G–**J,** Representative pictograms display TMEM assembly (white arrows). Whole BC specimens were immunostained for CD31 (blue), CD68 (green), MENA (red) and DAPI (grey), in (**G**). The TMEM score was assessed by quantifying 20 high-magnification fields/tumor section, visualized in (**H**), Pearson's correlation ($R^{2;}$ **p<0.01) between the TMEM score and VEGF-C-expressing TAMs in (**I**).

Statistical analyses were performed by one-way ANOVA in (**B**,**C**,**E** and **F**) and by Mann-Whitney U test in (**H**); **p<0.01 ***p<0.001, ****p<0.0001; n=4 for grade I, n=14 for grade II and 10 for grade III. Data are presented as the mean ± SD. Bars represent 100 µm in (**A**,**D**) and 20 µm in (**G**).

Figure 1

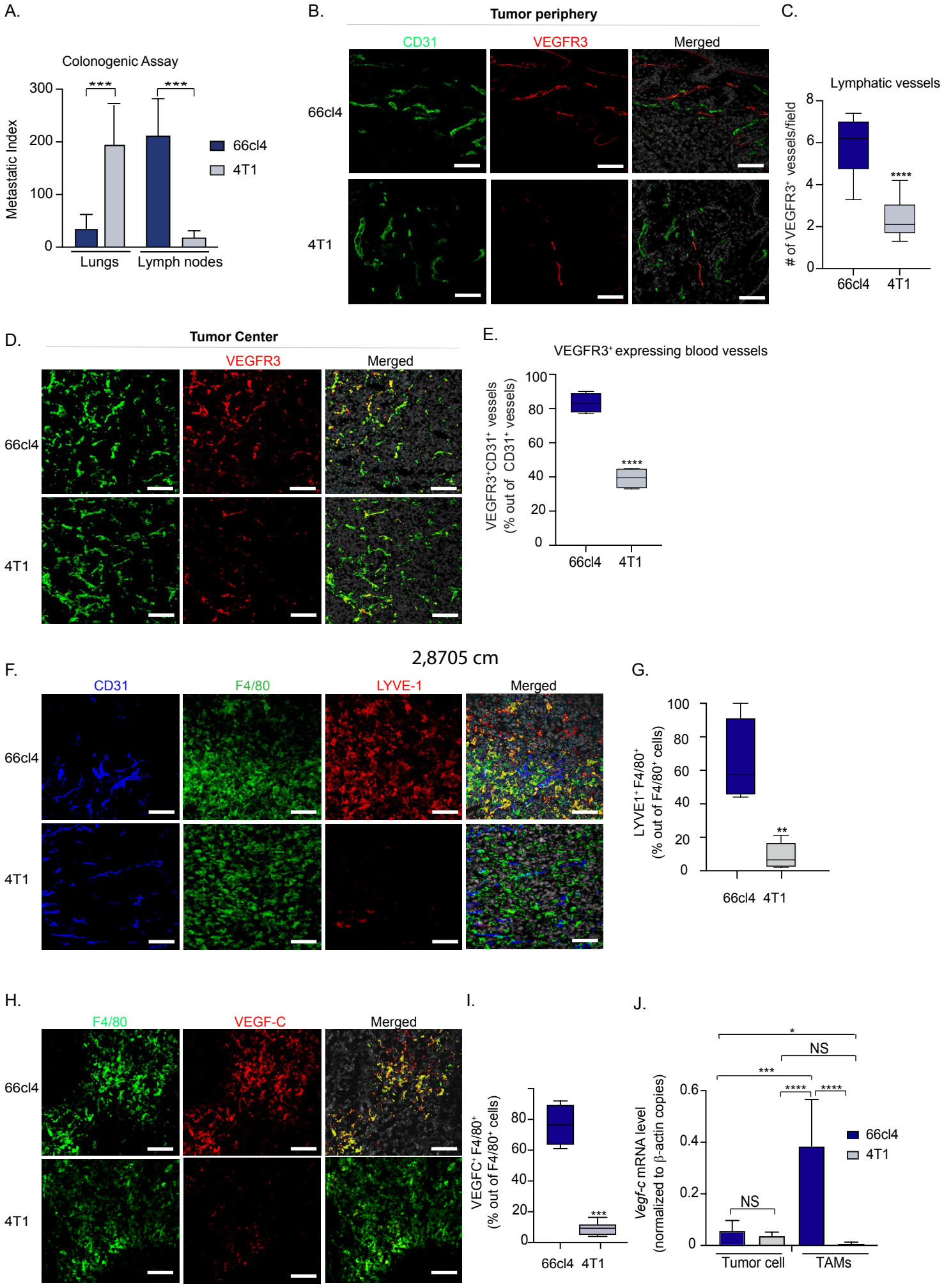
A.
Colonogenic Assay
Metastatic Index
300
200
100
0
***
***
66cl4
4T1
Lungs
Lymph nodes
B.
Tumor periphery
CD31
VEGFR3
Merged
66cl4
4T1
C.
Lymphatic vessels
# of VEGFR3+ vessels/field
8
6
4
2
0
****
66cl4
4T1
D.
Tumor Center
VEGFR3
Merged
66cl4
4T1
E.
VEGFR3+ expressing blood vessels
VEGFR3+CD31+ vessels
(% out of CD31+ vessels)
100
80
60
40
20
0
****
66cl4
4T1
F.
2,8705 cm
CD31
F4/80
LYVE-1
Merged
66cl4
4T1
G.
LYVE1+ F4/80+
(% out of F4/80+ cells)
100
80
60
40
20
0
**
66cl4
4T1
H.
F4/80
VEGF-C
Merged
66cl4
4T1
I.
VEGFC+ F4/80+
(% out of F4/80+ cells)
80
60
40
20
0
***
66cl4
4T1
J.
Vegf-c mRNA level
(normalized to β-actin copies)
0.6
0.4
0.2
0
*
NS
***
****
****
NS
66cl4
4T1
Tumor cell
TAMs

Figure 2

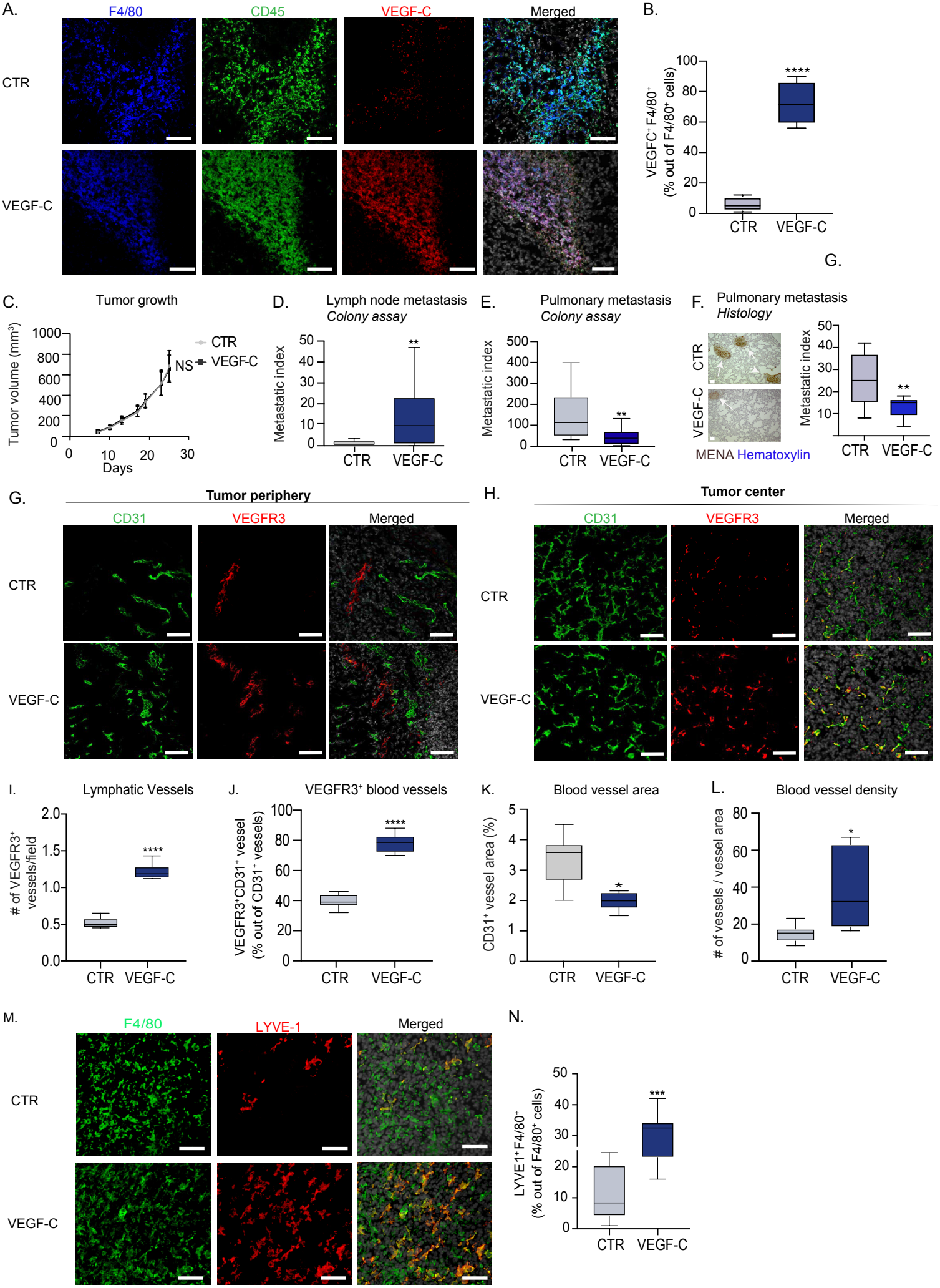
A.
F4/80
CD45
VEGF-C
Merged
CTR
VEGF-C
B.
VEGFC+ F4/80+ (% out of F4/80+ cells)
100
80
60
40
20
0
****
CTR
VEGF-C
G.
C.
Tumor growth
Tumor volume (mm3)
1000
800
600
400
200
0
0
10
20
30
Days
CTR
VEGF-C
NS
D.
Lymph node metastasis
Colony assay
Metastatic index
50
40
30
20
10
0
**
CTR
VEGF-C
E.
Pulmonary metastasis
Colony assay
Metastatic index
500
400
300
200
100
0
**
CTR
VEGF-C
F.
Pulmonary metastasis
Histology
CTR
VEGF-C
MENA Hematoxylin
Metastatic index
50
40
30
20
10
**
CTR
VEGF-C
G.
Tumor periphery
CD31
VEGFR3
Merged
CTR
VEGF-C
H.
Tumor center
CD31
VEGFR3
Merged
CTR
VEGF-C
I.
Lymphatic Vessels
# of VEGFR3+ vessels/field
2.0
1.5
1.0
0.5
0.0
****
CTR
VEGF-C
J.
VEGFR3+ blood vessels
VEGFR3+CD31+ vessel (% out of CD31+ vessels)
100
80
60
40
20
0
****
CTR
VEGF-C
K.
Blood vessel area
CD31+ vessel area (%)
5
4
3
2
1
0
*
CTR
VEGF-C
L.
Blood vessel density
# of vessels / vessel area
80
60
40
20
0
*
CTR
VEGF-C
M.
F4/80
LYVE-1
Merged
CTR
VEGF-C
N.
LYVE1+F4/80+ (% out of F4/80+ cells)
50
40
30
20
10
0
***
CTR
VEGF-C

Figure 3

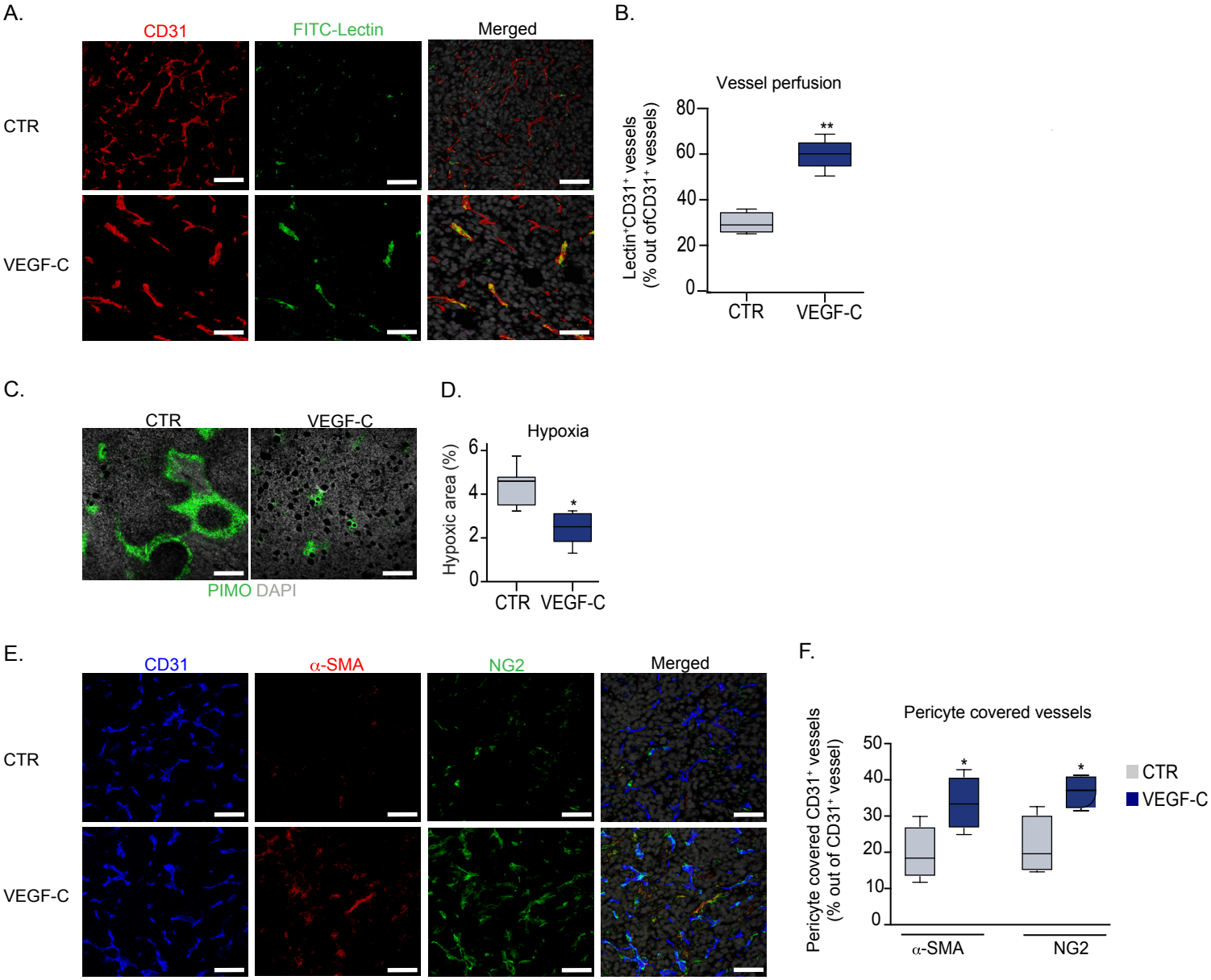
A.
CD31
FITC-Lectin
Merged
CTR
VEGF-C
B.
Vessel perfusion
Lectin+CD31+ vessels (% out ofCD31+ vessels)
80
60
40
20
0
**
CTR
VEGF-C
C.
CTR
VEGF-C
PIMO DAPI
D.
Hypoxia
Hypoxic area (%)
6
4
2
0
*
CTR
VEGF-C
E.
CD31
α-SMA
NG2
Merged
CTR
VEGF-C
F.
Pericyte covered vessels
Pericyte covered CD31+ vessels (% out of CD31+ vessel)
50
40
30
20
10
0
*
*
α-SMA
NG2
CTR
VEGF-C

Figure 4

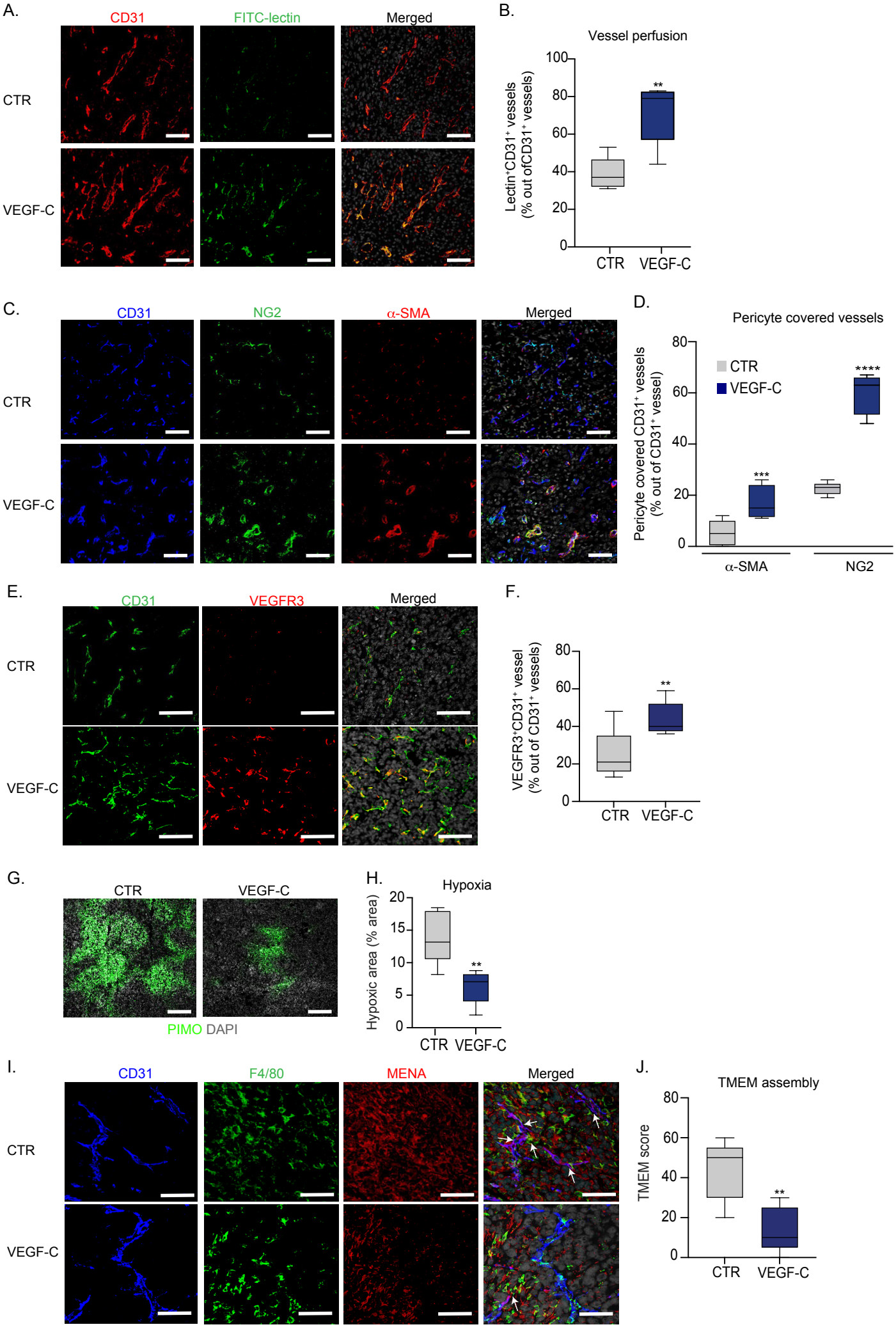
A.
CD31
FITC-lectin
Merged
CTR
VEGF-C
B.
Vessel perfusion
Lectin+CD31+ vessels (% out ofCD31+ vessels)
100
80
60
40
20
0
**
CTR
VEGF-C
C.
CD31
NG2
α-SMA
Merged
CTR
VEGF-C
D.
Pericyte covered vessels
Pericyte covered CD31+ vessels (% out of CD31+ vessel)
80
60
40
20
0
CTR
VEGF-C
***
****
α-SMA
NG2
E.
CD31
VEGFR3
Merged
CTR
VEGF-C
F.
VEGFR3+CD31+ vessel (% out of CD31+ vessels)
80
60
40
20
0
**
CTR
VEGF-C
G.
CTR
VEGF-C
PIMO DAPI
H.
Hypoxia
Hypoxic area (% area)
20
15
10
5
0
**
CTR
VEGF-C
I.
CD31
F4/80
MENA
Merged
CTR
VEGF-C
J.
TMEM assembly
TMEM score
80
60
40
20
0
**
CTR
VEGF-C

Figure 5

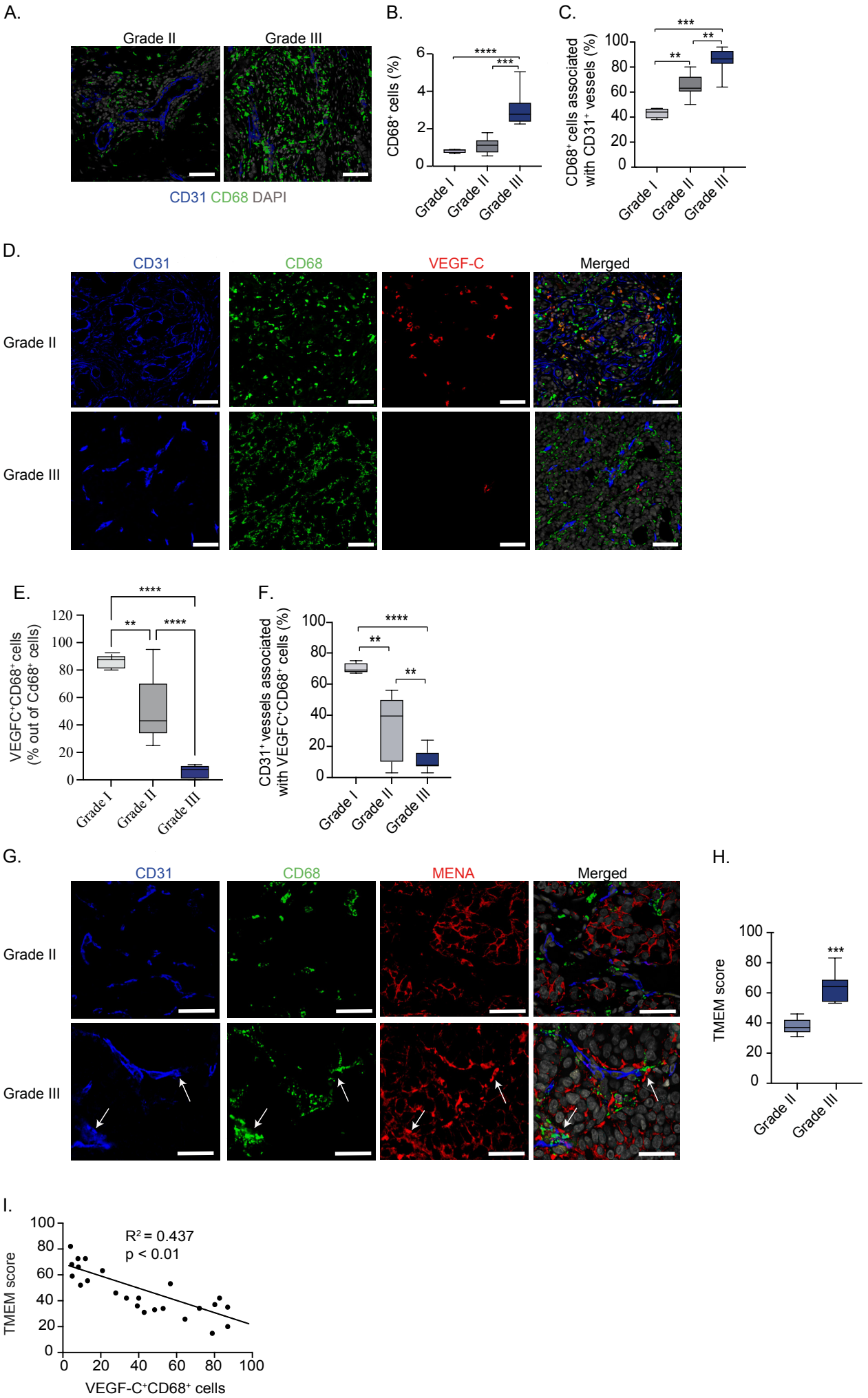
A.
Grade II
Grade III
CD31 CD68 DAPI
B.
CD68⁺ cells (%)
Grade I
Grade II
Grade III
C.
CD68⁺ cells associated with CD31⁺ vessels (%)
D.
CD31
CD68
VEGF-C
Merged
Grade II
Grade III
E.
VEGFC⁺CD68⁺ cells (% out of Cd68⁺ cells)
F.
CD31⁺ vessels associated with VEGFC⁺CD68⁺ cells (%)
G.
CD31
CD68
MENA
Merged
Grade II
Grade III
H.
TMEM score
I.
R² = 0.437
p < 0.01
TMEM score
VEGF-C⁺CD68⁺ cells

SUPPLEMENTAL FIGURE LEGENDS

Supplemental Figure 1. TAM-derived VEGF-C decreases lung metastases

66cl4 and 4T1 cancer cells were injected into the mammary fat pad of syngeneic mice.

A-B, 66cl4 and 4T1 tumor sections were immunostained for CD31 (green), Podoplanin (red) and F4/80 (green) in **(A)**. Graphs depict morphometric analysis of TAMs expressing Podoplanin in **(B).**

C, qPCR analysis of VEGF-A gene expression in flow cytometry-sorted TAMs or GFP^+ cancer cells from 4T1 and 66cl4 tumors is depicted in the graph.

D, Graph depicts morphometric analysis of $CD31^+$ vessel area (%).

E-F, Representative images for NG2 (green), α-SMA (red), CD31 (blue) and DAPI (grey) in (**E**). The graph displays morphometric analysis of pericyte covered blood vessels in ().

All images are quantified per optic field and bars represent 100 μm. Statistical analyses were performed by Students t-test for **(A,**), one-way ANOVA in (**C**) and by * indicates significance; *$p<0.05$; **$p<0.01$ ***$p<0.001$ $n>10$. Bars represent 100 μm. All data are presented as the mean + SD.

Supplemental Figure 2. VEGF-C integration levels and protein expression in hemopoietic cells

4T1 tumor cells were injected into the mammary fat pad of syngeneic chimeric mice harboring haemopoietic cells engineered to express VEGF-C or only the lentiviral backbone (CTRs).

A, Schematics describing the experimental procedure.

B, Genomic DNA was analyzed by qPCR for lentiviral integration of VEGF-C in bone marrow stem cells from CTR and VEGF-C chimeric mice. Histogram depicts lentiviral copies normalized to β-actin.

C, VEGF-C protein expression in BMDMs derived from CTR and VEGF-C chimeric mice was analyzed by western blot.

D, RT-PCR analysis of VEGF-A gene expression in BMDMs attained from CTR and VEGF-C chimeric mice.

E, Histogram depicts CTR and VEGF-C tumor weight (g).

F, The graph displays the metastatic index of blood tumor cell colonies (number of metastatic colonies in blood/g of primary tumor weight) of CTR or VEGF-C chimeric tumor bearing mice.

G, Graph depicts the number of $CD31^+$ vessels

H-J, Representative images show immunofluorescence staining of tumor sections from CTR and VEGF-C chimeric mice for Podoplanin (red) and F4/80 (green). Graph depicts morphometric analysis of Podoplanin expressing TAMs in (**G**).

All images are quantified per optic field and bars represent 100 µm. Statistical analyses were performed by Students t-test, *indicates significance; *$p<0.05$; ****$p<0.001$, $n>15$. All data are presented as the mean + SD.

Supplemental Figure 3. TAM-derived VEGF-C decreases vessel permeability

4T1 cancer cells were co-mingled in matrigel with BMDMs transduced with CTR or VEGF-C LVs and injected subcutaneously into syngeneic mice.

A, Schematic figure of the co-mingling assay

B, CTR and VEGF-C tumor sections were immunostained for CD31 (green), biotin conjugated dextran (red). Bars represent 100 µm. Vessel leakage is defined as extravasating dextran as visualized in the graph (n=5; ****$p<0.0001$ * indicates significance by students t-test).

Supplemental Figure 4. TAM-derived VEGF-C does not the affect myeloid and lymphoid immune landscape

A-F, Graphs show flow cytometry analysis of 4T1-CTR and 4T1-VEGF-C tumors for myeloid cells in (**A**), TAMs in (**B**), neutrophils in (**C**), immunostimulatory TAMs in (**E**), immunosuppressive TAMs in (**F**).

G, Graph displays quantitative RT-PCR analysis of gene expression levels of CTR and VEGF-C transduced BMDMs. Gene expression was normalized to β-actin levels.

H, Flow cytometry analysis of 4T1-CTR and 4T1-VEGF-C tumors for T cells and NK cells.

All statistical analyses in were performed by Students t-test, and was not significant, $n>15$. All data represents are presented as the mean + SD.

Supplemental Figure 5. Vessel number is not changed with BC grade

The graph depicts morphometric analysis of BC specimens of grades II and III immunostained for CD31, $n>4$-16. Statistical analysis by students t-test was not significant (NS).

Supplemental Figure 1

A.

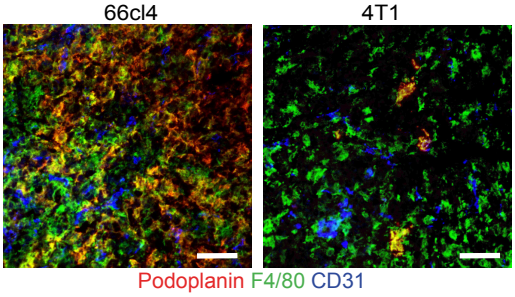

B.

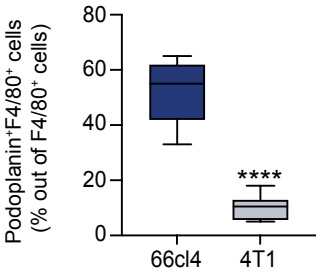

C.

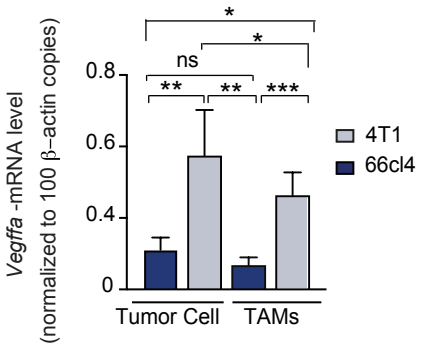

D.

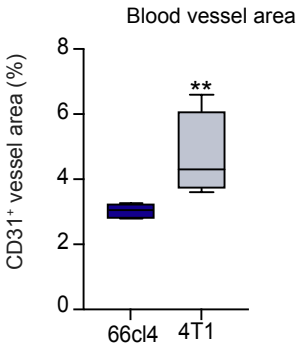

E.

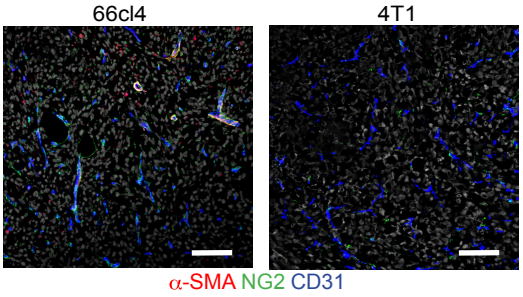

F.

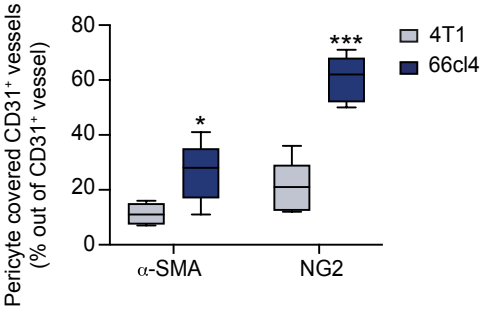

Supplemental Figure 2

A.

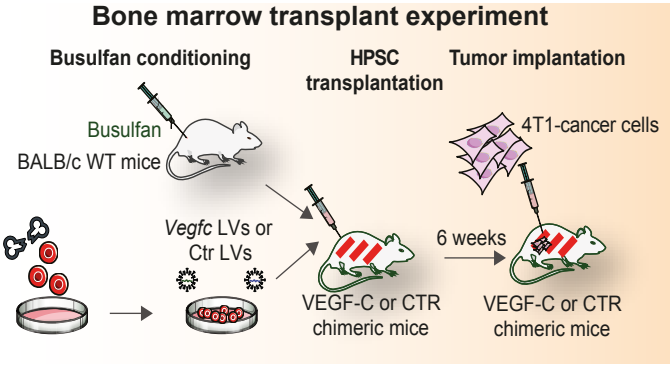

B.

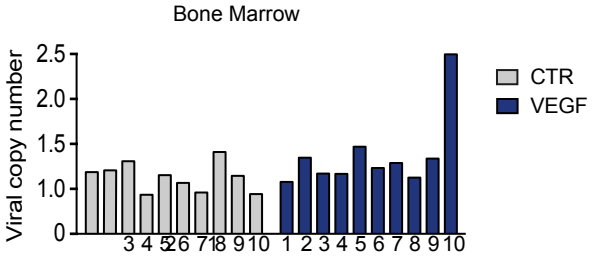

C.

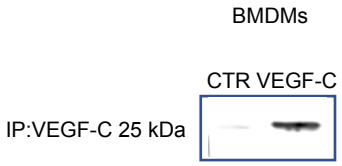

D.

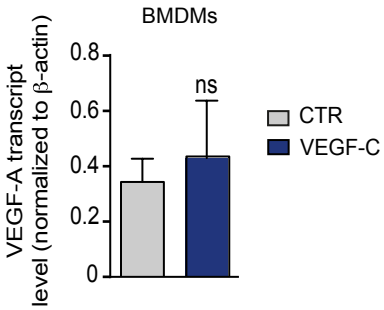

E.

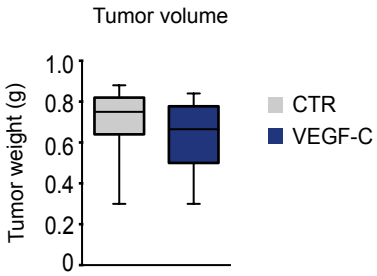

F.

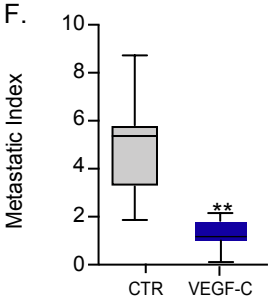

H.

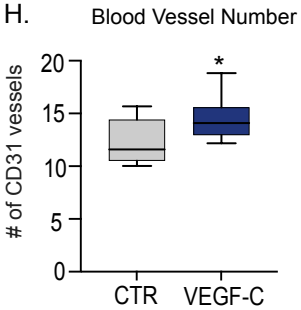

I.

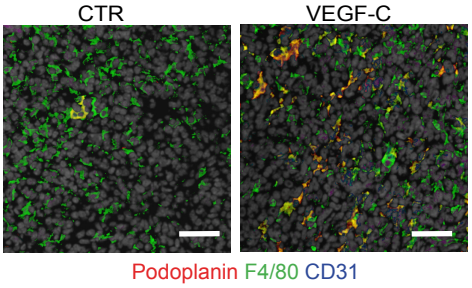

J.

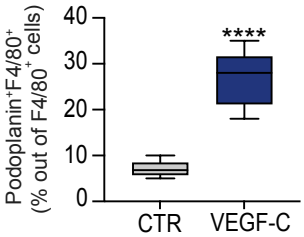

Supplemental Figure 3

A.

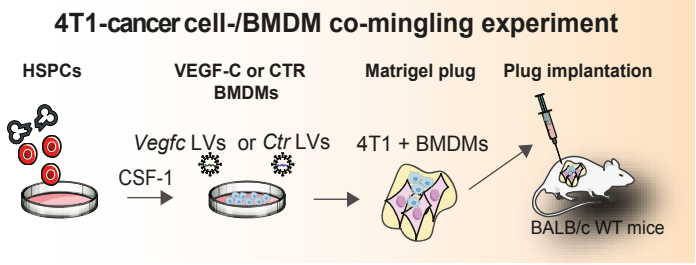

B.

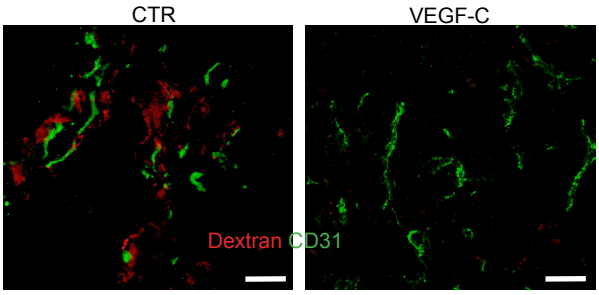

C.

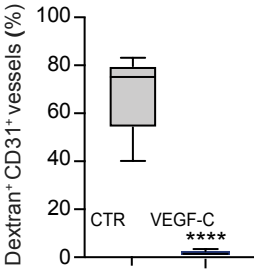

Supplemental Figure 4

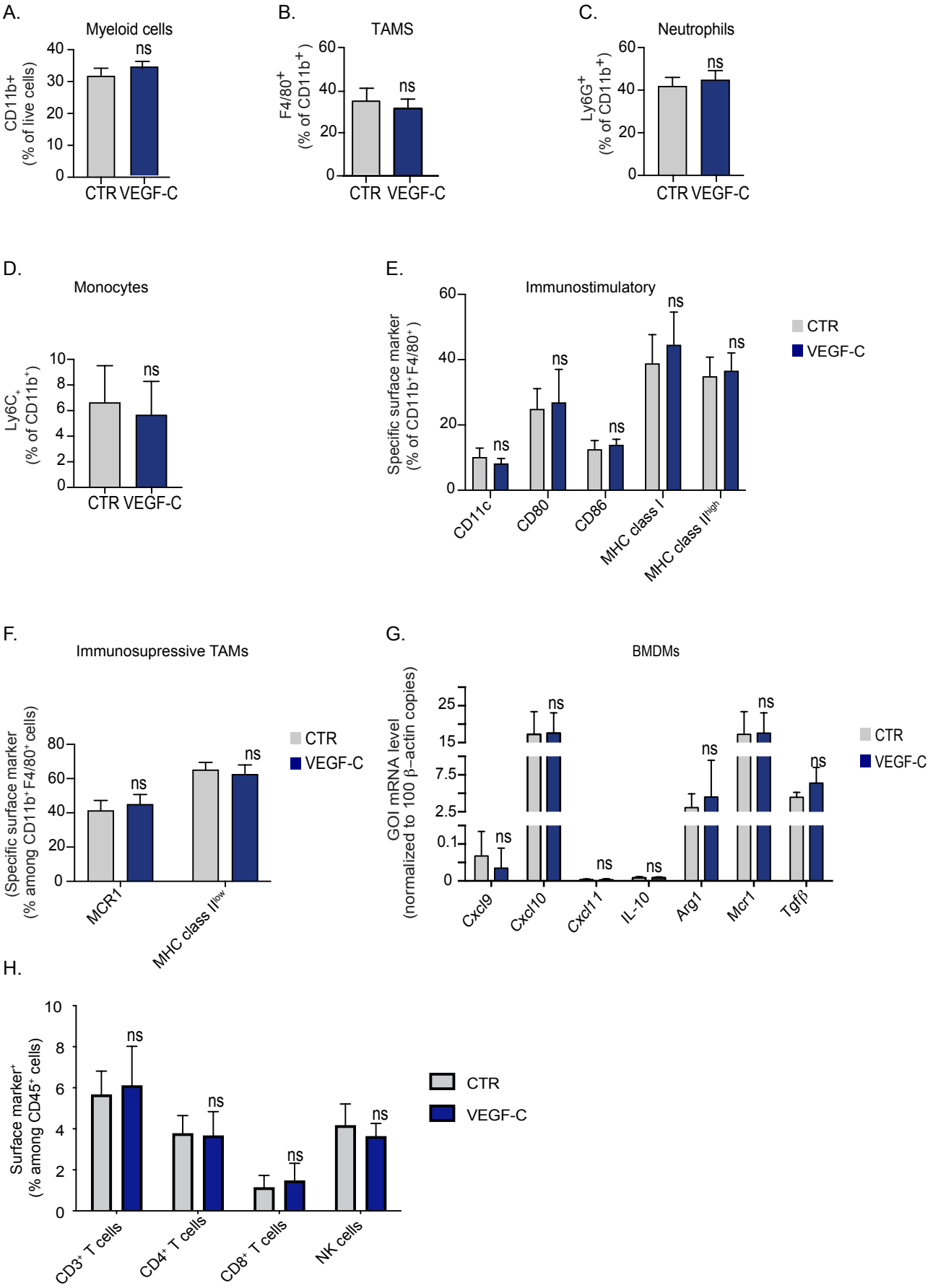

SUPPLEMENTAL FIGURE LEGENDS

Supplemental Figure 1. TAM-derived VEGF-C decreases lung metastases

66cl4 and 4T1 cancer cells were injected into the mammary fat pad of syngeneic mice.

A-B, 66cl4 and 4T1 tumor sections were immunostained for CD31 (green), Podoplanin (red) and F4/80 (green) in **(A)**. Graphs depict morphometric analysis of TAMs expressing Podoplanin in **(B).**

C, qPCR analysis of VEGF-A gene expression in flow cytometry-sorted TAMs or GFP^+ cancer cells from 4T1 and 66cl4 tumors is depicted in the graph.

D, Graph depicts morphometric analysis of $CD31^+$ vessel area (%).

E-F, Representative images for NG2 (green), α-SMA (red), CD31 (blue) and DAPI (grey) in (**E**). The graph displays morphometric analysis of pericyte covered blood vessels in ().

All images are quantified per optic field and bars represent 100 μm. Statistical analyses were performed by Students t-test for **(A,**), one-way ANOVA in (**C**) and by * indicates significance; *$p<0.05$; **$p<0.01$ ***$p<0.001$ $n>10$. Bars represent 100 μm. All data are presented as the mean + SD.

Supplemental Figure 2. VEGF-C integration levels and protein expression in hemopoietic cells

4T1 tumor cells were injected into the mammary fat pad of syngeneic chimeric mice harboring haemopoietic cells engineered to express VEGF-C or only the lentiviral backbone (CTRs).

A, Schematics describing the experimental procedure.

B, Genomic DNA was analyzed by qPCR for lentiviral integration of VEGF-C in bone marrow stem cells from CTR and VEGF-C chimeric mice. Histogram depicts lentiviral copies normalized to β-actin.

C, VEGF-C protein expression in BMDMs derived from CTR and VEGF-C chimeric mice was analyzed by western blot.

D, RT-PCR analysis of VEGF-A gene expression in BMDMs attained from CTR and VEGF-C chimeric mice.

E, Histogram depicts CTR and VEGF-C tumor weight (g).

F, The graph displays the metastatic index of blood tumor cell colonies (number of metastatic colonies in blood/g of primary tumor weight) of CTR or VEGF-C chimeric tumor bearing mice.

G, Graph depicts the number of $CD31^+$ vessels

H-J, Representative images show immunofluorescence staining of tumor sections from CTR and VEGF-C chimeric mice for Podoplanin (red) and F4/80 (green). Graph depicts morphometric analysis of Podoplanin expressing TAMs in (**G**).

All images are quantified per optic field and bars represent 100 µm. Statistical analyses were performed by Students t-test, *indicates significance; *$p<0.05$; ****$p<0.001$, $n>15$. All data are presented as the mean + SD.

Supplemental Figure 3. TAM-derived VEGF-C decreases vessel permeability

4T1 cancer cells were co-mingled in matrigel with BMDMs transduced with CTR or VEGF-C LVs and injected subcutaneously into syngeneic mice.

A, Schematic figure of the co-mingling assay

B, CTR and VEGF-C tumor sections were immunostained for CD31 (green), biotin conjugated dextran (red). Bars represent 100 µm. Vessel leakage is defined as extravasating dextran as visualized in the graph (n=5; ****$p<0.0001$ * indicates significance by students t-test).

Supplemental Figure 4. TAM-derived VEGF-C does not the affect myeloid and lymphoid immune landscape

A-F, Graphs show flow cytometry analysis of 4T1-CTR and 4T1-VEGF-C tumors for myeloid cells in (**A**), TAMs in (**B**), neutrophils in (**C**), immunostimulatory TAMs in (**E**), immunosuppressive TAMs in (**F**).

G, Graph displays quantitative RT-PCR analysis of gene expression levels of CTR and VEGF-C transduced BMDMs. Gene expression was normalized to β-actin levels.

H, Flow cytometry analysis of 4T1-CTR and 4T1-VEGF-C tumors for T cells and NK cells.

All statistical analyses in were performed by Students t-test, and was not significant, $n>15$. All data represents are presented as the mean + SD.

Supplemental Figure 5. Vessel number is not changed with BC grade

The graph depicts morphometric analysis of BC specimens of grades II and III immunostained for CD31, $n>4$-16. Statistical analysis by students t-test was not significant (NS).

Supplemental Figure 1

A.

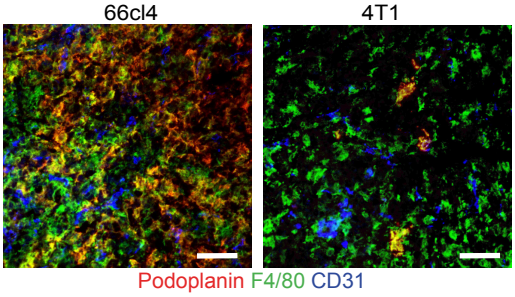

B.

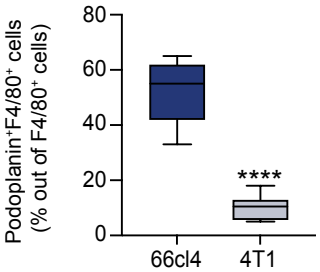

C.

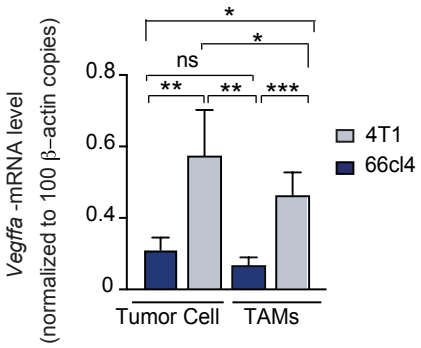

D.

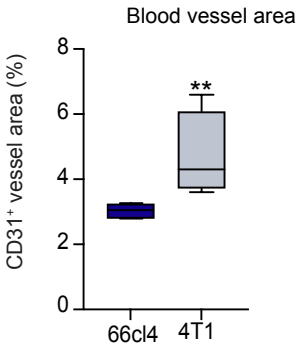

E.

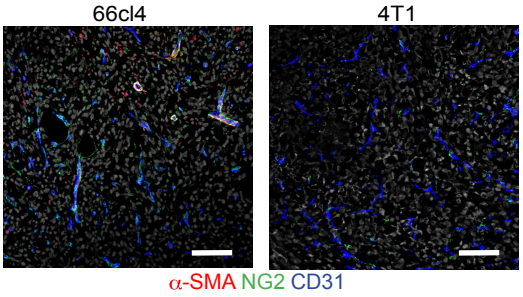

F.

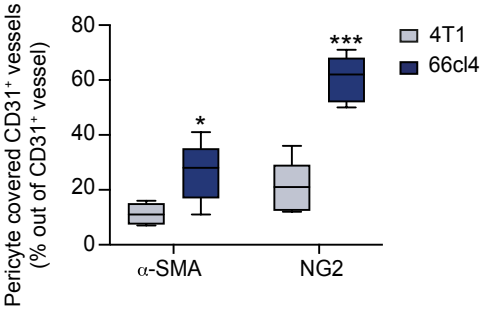

Supplemental Figure 2

A.

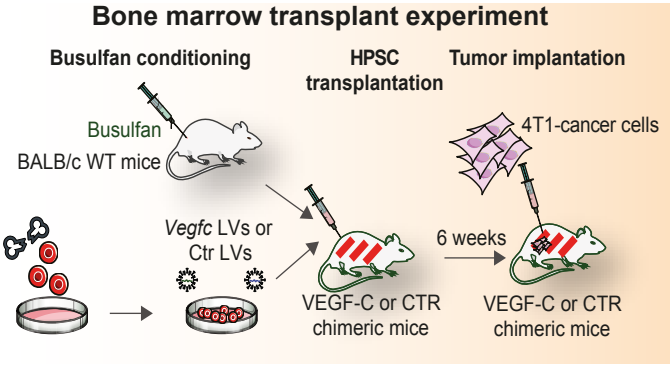

B.

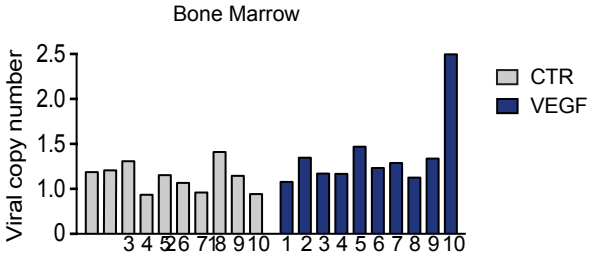

C.

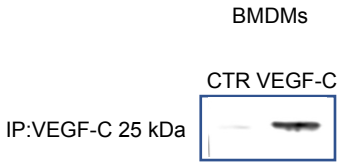

D.

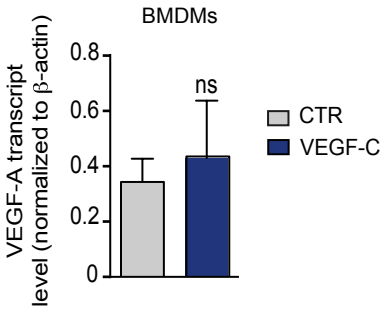

E.

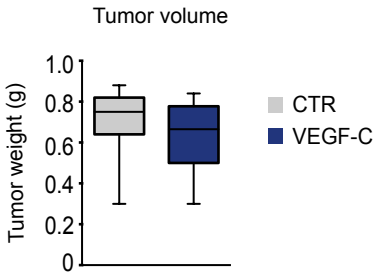

F.

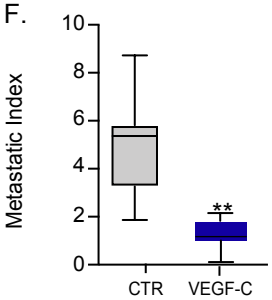

H.

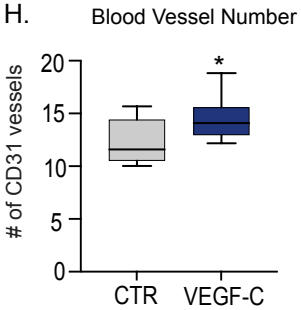

I.

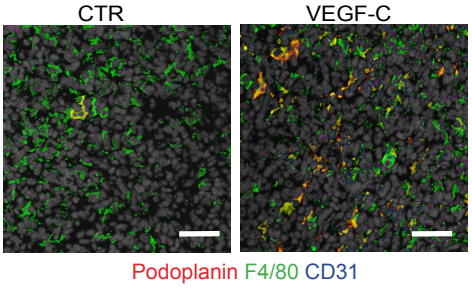

J.

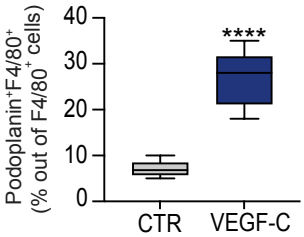

Supplemental Figure 3

A.

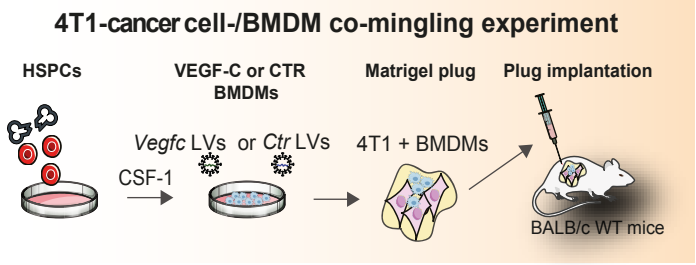

B.

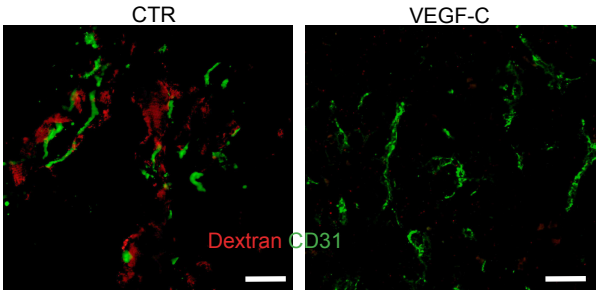

C.

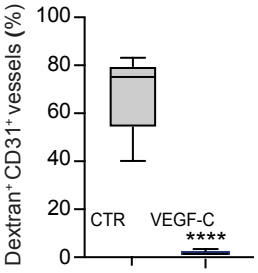
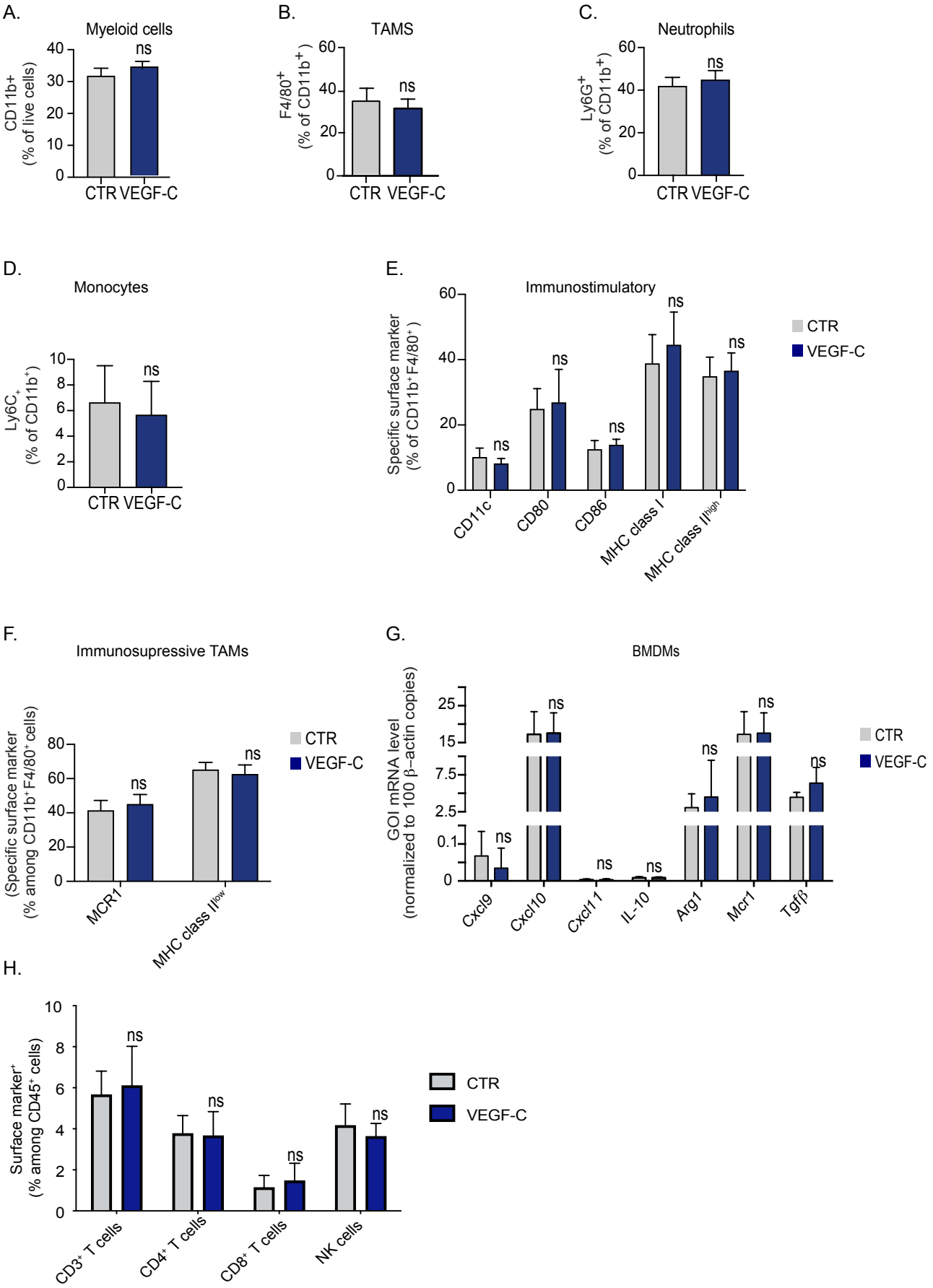
Supplemental Figure 4